cmgh
CELLULAR AND MOLECULAR GASTROENTEROLOGY AND HEPATOLOGY

ORIGINAL RESEARCH

# Macrophage SCAP Contributes to Metaflammation and Lean NAFLD by Activating STING–NF-κB Signaling Pathway

Xinyu Huang,[1,*] Yingcheng Yao,[1,*] Xiaoli Hou,[1,*] Li Wei,[1] Yuhan Rao,[1] Yu Su,[1] Guo Zheng,[1] Xiong Z. Ruan,[1,2] Danyang Li,[1] and Yaxi Chen[1]

[1]Centre for Lipid Research & Key Laboratory of Molecular Biology for Infectious Diseases (Ministry of Education), Institute for Viral Hepatitis, Department of Infectious Diseases, Second Affiliated Hospital, Chongqing Medical University, Chongqing, China; and [2]John Moorhead Research Laboratory, Centre for Nephrology, University College London Medical School, Royal Free Campus, University College London, London, United Kingdom

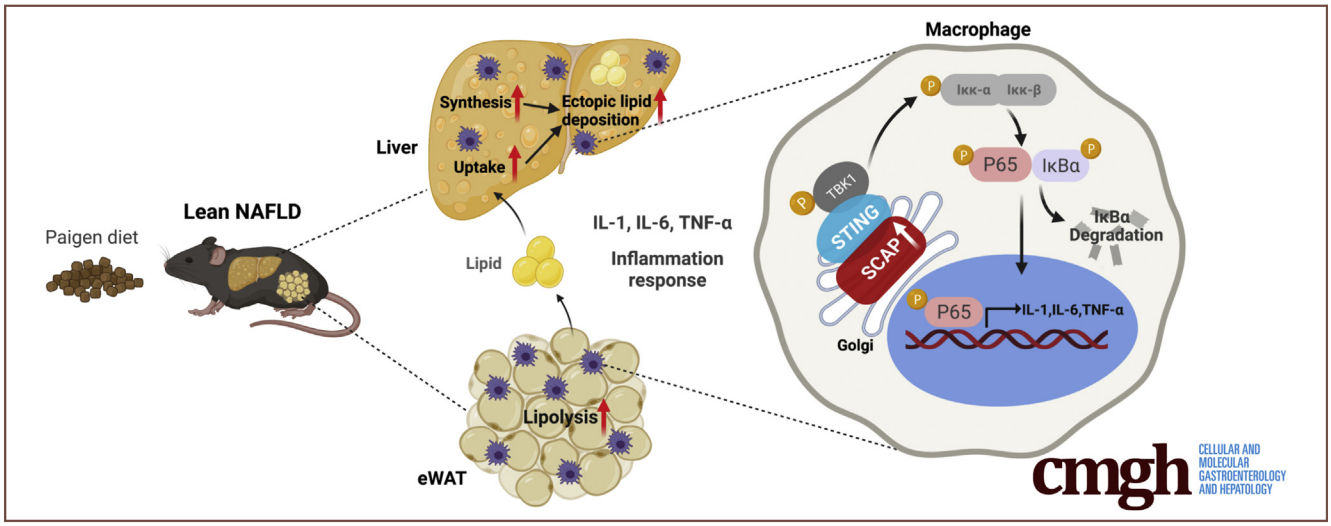


## SUMMARY

In the mouse model of lean NAFLD induced by Paigen diet, macrophage SCAP was abnormally increased and led to severe metaflammation through activating STING–NF-κB signaling pathway. The metaflammation increased lipolysis in the adipose and enhanced hepatic lipid uptake and synthesis, consequently resulting in ectopic lipid deposition in the liver and hepatic injury.

**BACKGROUND & AIMS:** Sterol regulatory element binding protein cleavage-activating protein (SCAP) is a cholesterol sensor that confers a broad range of functional effects in metabolic diseases. Lean nonalcoholic fatty liver disease (NAFLD) is characterized by a decrease in subcutaneous fat and ectopic fat deposition in the liver. SCAP may mediate the development of lean NAFLD, but the mechanism of action remains unclear.

**METHODS:** C57BL/6J wild-type and macrophage SCAP-specific knockout mice ($SCAP^{\Delta M\varphi}$) were subjected to Paigen diet (PD) feeding induced lean NAFLD. Inflammation and lipid metabolism of adipose and liver were evaluated. The STING–NF-κB signaling pathway was examined in vivo and in vitro to explore the underlying mechanism of macrophage SCAP on metaflammation.

**RESULTS:** The data showed heterogeneity of lipid metabolic processes in liver and epididymal white adipose tissue due to inflammation mediated by macrophage infiltration. Meanwhile, we found that the macrophage SCAP was abnormally increased in the adipose and liver tissues of PD-fed mice. Intriguingly, the $SCAP^{\Delta M\varphi}$ mice attenuated PD-induced metaflammation and ectopic lipid deposition by reducing hepatic stimulator of interferon gene (STING)–nuclear factor kappa B (NF-κB) pathway activation. In-depth molecular analysis revealed that SCAP specifically recruits the STING and tank-binding kinase 1 onto the Golgi to activate the NF-κB in macrophages, thereby promoting the release of inflammatory factors. This process ultimately led to an increased lipolysis in adipocytes and lipid uptake and synthesis in hepatocytes.

**CONCLUSIONS:** Our findings suggest that SCAP acts as a novel regulator of the macrophage inflammatory response and the pathogenesis of lean NAFLD by activating the STING–NF-κB signaling pathway. Inhibition of macrophage SCAP may represent a new therapeutic strategy for the treatment of lean NAFLD. *(Cell Mol Gastroenterol Hepatol 2022;14:1–26; https://doi.org/10.1016/j.jcmgh.2022.03.006)*

*Keywords:* Lean NAFLD; SCAP; Paigen Diet; Metaflammation; STING-NF-κB Pathway.

Nonalcoholic fatty liver disease (NAFLD) is commonly considered to be associated with obesity. However, NAFLD has also been increasingly reported in persons with lean NAFLD, with a body mass index (BMI) <25 kg/m$^2$ for Western subjects and BMI <23 kg/m$^2$ for Eastern subjects.[1] The current rate of nonobese NAFLD is 36%–45%, and lean NAFLD is 7%–23% in the global NAFLD population,[1–4] and the morbidity of lean NAFLD in Eastern countries is much higher than that of Western countries.[4–7] Lean NAFLD is defined as a "metabolically unhealthy normal weight" NAFLD, which is characterized by a decrease in subcutaneous fat and ectopic fat deposition in the liver. Thus, the location and type of obesity have a more significant impact on an individual's metabolic health than the total mass of fat.[8] Although patients with lean NAFLD are not obese, they are still susceptible to metabolic syndrome, similar to that of obese NAFLD.[9,10] There are reports that lean NAFLD has an increased risk for the development and progression of severe liver disease.[11,12] The pathogenesis of lean NAFLD appears complex and is still poorly understood.

Compared with obese patients, adipose tissue dysfunction of patients with lean NAFLD exhibits a higher adverse adipokine profile, ultimately leading to systemic chronic low-grade inflammation, also known as metaflammation.[13,14] Moreover, enriched cholesterol dietary patterns cause disturbances in the intestinal microbial environment, which may be necessary for the progression of lean NAFLD.[15–17] These phenomena are almost consistent with another study that shows the use of a cholesterol-rich Paigen diet (PD) to induce a NAFLD model with weight loss and significant systemic inflammation.[18] Consequently, it is reasonable to speculate that cholesterol homeostasis and metaflammation play critical roles in the pathogenesis of lean NAFLD.

Sterol regulatory element binding protein (SREBP) cleavage-activating protein (SCAP) is a cholesterol sensor that regulates signal transduction for intracellular cholesterol homeostasis.[19,20] Dysregulation of SCAP could affect the development of metabolic disease. Our previous studies demonstrated that inflammatory factors increase the expression of SCAP and promote the translocation of the SCAP/SREBP2 complex from the endoplasmic reticulum (ER) to the Golgi, which destroys intracellular cholesterol homeostasis and leads to atherosclerosis[21,22] and NAFLD.[23] We also discovered that crosstalk between the SCAP/SREBP and TLR4-MyD88-NF-κB inflammatory pathways mediates macrophage foam cell formation in atherosclerosis.[24,25] Moreover, we found that SCAP overexpression promotes SCAP and NLRP3 inflammasome translocation to the Golgi and increases the activation of the NLRP3 inflammasome pathway, consequently accelerating atherosclerosis.[26] These findings suggest that SCAP is a crucial bridge molecule connecting lipid metabolism and inflammation, which represents an attractive target for the treatment of metabolic diseases. In view of the important role of SCAP in regulating cholesterol metabolism and inflammation, we hypothesize that the abnormal function of SCAP may result in the occurrence of lean NAFLD.

In this study, we successfully established a metabolic disease model characterized by lean NAFLD using a PD. Mice fed with PD developed clear weight loss and ectopic lipid deposition in the liver, accompanied by increased SCAP expression in macrophages of adipose and liver tissue. In contrast, knockout of macrophage SCAP (SCAP$^{\Delta M\varphi}$) in mice attenuated PD-induced metaflammation and ectopic lipid deposition. Mechanistically, macrophage SCAP deletion reduced adipose tissue and liver metaflammation by inhibiting stimulator of interferon gene (STING)/tank-binding kinase 1 (TBK1)–mediated nuclear factor kappa B (NF-κB) inflammatory signaling activation, consequently improving metabolic syndrome. Our findings provide new mechanistic insight into the pathogenesis of lean NAFLD, suggesting that inhibition of macrophage-specific expression of SCAP might be a potential therapeutic target for patients with lean NAFLD.

## Results

### *Nonobese Metabolic Syndrome Induced by PD Feeding Features Lean NAFLD*

After C57/BL6 mice were fed either normal chow (NCD) or PD for 12 weeks, compared with the NCD control group, the body weight of the mice was clearly decreased in the PD-fed group (Figure 1*A*), which was accompanied by marked manifestations of metabolic syndrome, hyperlipidemia, impaired glucose tolerance, and insulin sensitivity (Figure 1*B*–*D*). To clarify the cause of weight loss in PD-fed mice, we evaluated the weight of critical internal organs. PD-fed mice displayed increased liver weight with significant reduction in epididymal white adipose tissue (eWAT) weight (Figure 1*E* and *F*). Further analysis of these 2 organs revealed evident morphologic alterations in tissue architecture. H&E staining showed that adipocytes were smaller

*Authors share co-first authorship.

***Abbreviations used in this paper:*** **ALT, alanine aminotransferase; BMI, body mass index; Co-IP, co-immunoprecipitation; DMEM, Dulbecco modified Eagle medium; ER, endoplasmic reticulum; eWAT, epididymal white adipose tissue; FBS, fetal bovine serum; GTT, glucose tolerance test; 25-HC, 25-hydroxycholesterol; HDL, high-density lipoprotein; IKK, IκB kinase; IL, interleukin; ITT, insulin tolerance test; LPS, lipopolysaccharide; LDL, low-density lipoprotein; MCP-1, monocyte chemoattractant protein-1; NAFLD, nonalcoholic fatty liver disease; NCD, normal chow diet; NF-κB, nuclear factor kappa B; PBS, phosphate-buffered saline; PD, Paigen diet; qRT-PCR, quantitative real-time polymerase chain reaction; SCAP, sterol regulatory element binding protein cleavage-activating protein; SD, standard deviation; SREBP, sterol regulatory element binding protein; STING, stimulator of interferon gene; TBK1, tank-binding kinase 1; TC, total cholesterol; TG, triglyceride; TNF, tumor necrosis factor.**

**Most current article**



2352-345X
https://doi.org/10.1016/j.jcmgh.2022.03.006

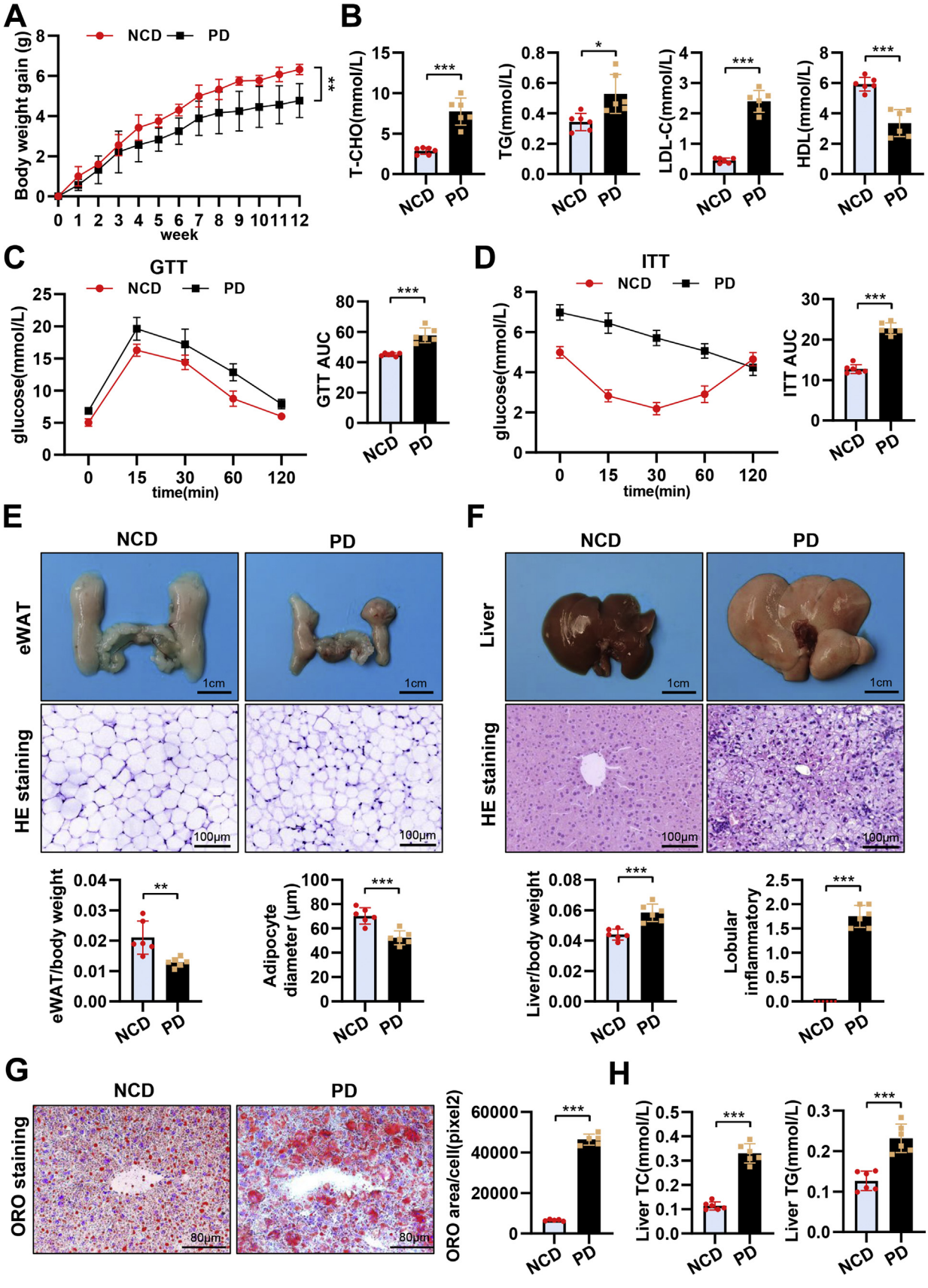
A
NCD
PD
Body weight gain (g)
week
**
B
T-CHO(mmol/L)
TG(mmol/L)
LDL-C(mmol/L)
HDL(mmol/L)
***
*
NCD
PD
C
GTT
glucose(mmol/L)
time(min)
GTT AUC
D
ITT
ITT AUC
E
eWAT
HE staining
1cm
100μm
eWAT/body weight
Adipocyte diameter (μm)
F
Liver
Liver/body weight
Lobular inflammatory
G
ORO staining
80μm
ORO area/cell(pixel2)
H
Liver TC(mmol/L)
Liver TG(mmol/L)

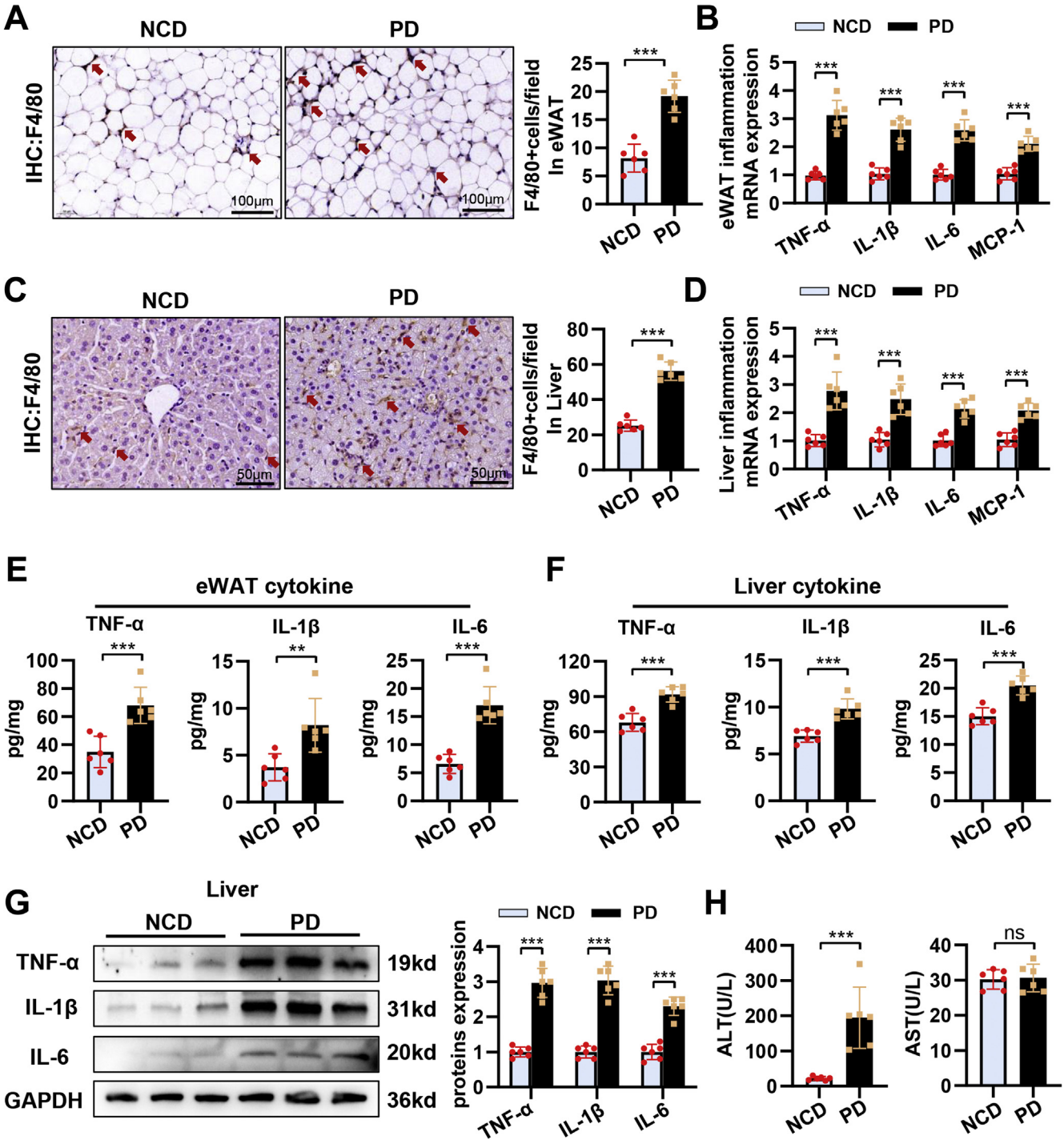


**Figure 2. Lean NAFLD induced by PD feeding displays evident inflammation in eWAT and liver.** (*A*) Immunohistochemical staining of F4/80$^{+}$ cells in eWAT (n = 6). (*B*) Relative mRNA levels of IL1$\beta$, IL6, TNF-$\alpha$, and MCP-1 in eWAT (n = 6). (*C*) Immunohistochemical staining of F4/80$^{+}$ cells in liver tissues (n = 6). (*D*) Relative mRNA levels of IL1$\beta$, IL6, TNF-$\alpha$, and MCP-1 in liver tissues (n = 6). Enzyme-linked immunosorbent assay analysis of protein expression of IL1$\beta$, IL6, and TNF-$\alpha$ in eWAT (*E*) and in liver tissues (*F*) (n = 6). (*G*) Protein levels of TNF-$\alpha$, IL1$\beta$, and IL6 in liver tissues (n = 6). (*H*) Levels of ALT and aspartate aminotransferase in plasma (n = 6). Data are expressed as mean ± SD. *$P < .05$; **$P < .01$; ***$P < .0001$; ns, nonsignificant (2-tailed unpaired *t* test in bar graphs).

**Figure 1.** (***See previous page***). **Nonobese metabolic syndrome induced by PD feeding features lean NAFLD.** (*A*) Body weight gain curves of mice fed 12-week NCD and PD (n = 6). (*B*) Levels of total TG, TC, HDL cholesterol, and LDL in plasma (n = 6). Intraperitoneal GTT levels (*C*) and intraperitoneal ITT levels (*D*) in NCD- and PD-fed mice (n = 6). (*E*) Representative pictures and H&E staining of eWAT, and the histogram represents eWAT/body weight (n = 6). (*F*) Representative pictures and H&E staining of liver tissues, and the histogram represents liver/body weight (n = 6). (*G*) Representative images of Oil Red O staining in liver tissues (n = 6). (*H*) Levels of intrahepatic TC and TG (n = 6). Data are expressed as mean ± SD. *$P < .05$; **$P < .01$; ***$P < .0001$; ns, nonsignificant (2-tailed unpaired *t* test in bar graphs and two-way analysis of variance in body weight, GTT, and ITT curves).

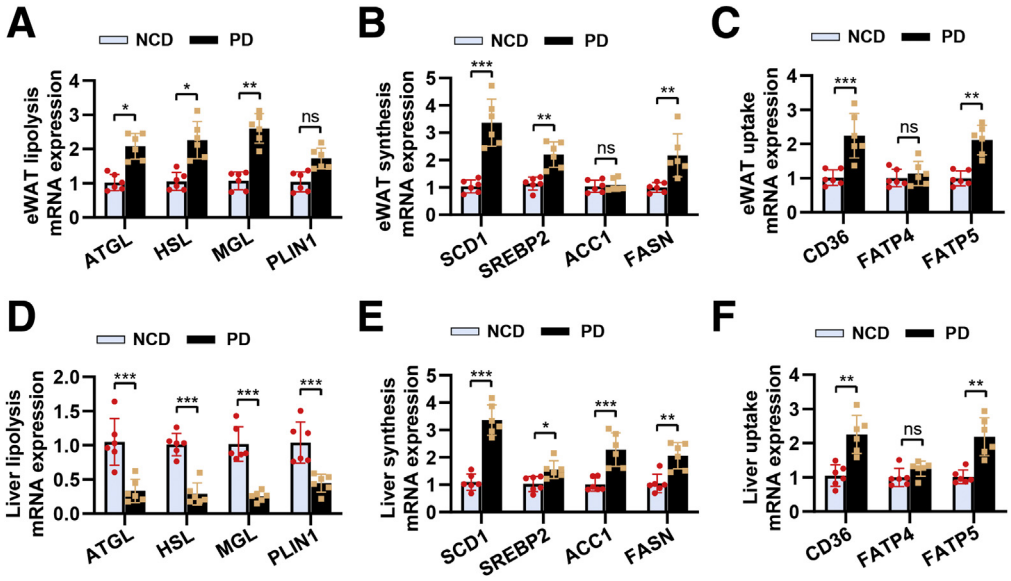


**Figure 3. Lean NAFLD induced by PD feeding displays evident lipid metabolism disorders in eWAT and liver.** Relative mRNA levels of lipolysis (*A*), lipid synthesis (*B*), and lipid uptake (*C*) in eWAT (n = 6). Relative mRNA levels of lipolysis (*D*), lipid synthesis (*E*), and lipid uptake (*F*) in liver tissues (n = 6). Data are expressed as mean ± SD. $^{*}P < .05$; $^{**}P < .01$; $^{***}P < .0001$; ns, nonsignificant (2-tailed unpaired *t* test in bar graphs).

in eWAT, and hepatocyte steatosis and lobular inflammatory infiltration were clearer in the PD-fed mice than in NCD-fed mice (Figure 1*E* and *F*). Meanwhile, Oil Red O staining showed obvious intracellular hepatocyte accumulation of neutral lipids in the PD-fed mice (Figure 1*G*). Increased intrahepatic total cholesterol (TC) and triglyceride (TG) contents confirmed these morphologic changes in liver of PD-fed mice (Figure 1*H*). These data indicate that nonobese metabolic syndrome induced in PD-fed mice features lean NAFLD, hyperlipidemia, glucose intolerance, and impaired insulin sensitivity.

## *Lean NAFLD Induced by PD Feeding Displays Evident Inflammation and Lipid Metabolism Disorders in eWAT and Liver*

Previous studies indicated that PD-fed mice had more severe systemic inflammation.[18] We observed similar phenomena in the mouse models. Our data showed that macrophages significantly infiltrated in eWAT and liver tissues of the PD-fed mice. The expression and secretion of interleukin (IL) 1$\beta$, IL6, tumor necrosis factor (TNF) $\alpha$, and monocyte chemoattractant protein-1 (MCP-1) were increased in both tissues of PD-fed mice (Figure 2*A*–*G*). Meanwhile, plasma alanine aminotransferase (ALT) levels were significantly elevated in the PD-fed mice (Figure 2*H*).

Because the subtle balance among lipid uptake, synthesis, and lipolysis is relevant for intracellular lipid content in adipocytes and hepatocytes, we further examined the mRNA levels of key genes of lipid metabolism. Interestingly, we found that eWAT and liver tissues exhibited different phenotypes of lipid metabolism disorders under PD-induced inflammation state; the adipose tissue was characterized by increased lipolysis (ATGL, HSL, and MGL mRNA were significantly up-regulated), synthesis (SCD1, SREBP2, and FASN mRNA were increased), and lipid uptake (CD36 and FATP5 mRNA were increased) (Figure 3*A*–*C*). However, the liver was characterized by decreased lipolysis (ATGL, HSL, MGL, and PLIN1 mRNA were significantly down-regulated) and increased synthesis (SCD1, SREBP2, ACC1, and FASN mRNA were increased) and lipid uptake (CD36 and FATP5 mRNA were increased) (Figure 3*D*–*F*). These data suggest that PD-induced inflammation in the liver and eWAT, as well as consequent different features of lipid disorders between the organs, is a critical process in the pathogenesis of lean NAFLD.

## *Macrophage SCAP Expression Is Abnormally Increased in eWAT and Liver Tissues of PD-Fed Mice*

Systemic inflammation and dysregulation of metabolic homeostasis are the key events in the initiation of lean NAFLD. SCAP has been previously documented as a signaling hub integrating cholesterol metabolism with inflammation in macrophages. We further observed the expression of macrophage SCAP in PD-fed mice. Macrophage SCAP expression was higher in the eWAT and liver tissues of PD-fed mice using the detection method of immunofluorescence and flow cytometry (Figure 4*A*–*C*). To conclusively establish the role of abnormally activated macrophage SCAP in lean NAFLD, we generated macrophage/monocyte-specific SCAP knockout mice LysM-Cre$^{+}$SCAP$^{fl/fl}$ (SCAP$^{\Delta M\varphi}$). The genotype of mice was determined by polymerase chain reaction using tail tissues. Successful deletion of macrophage SCAP in SCAP$^{\Delta M\varphi}$ mice was confirmed by quantitative real-time polymerase chain reaction (qRT-PCR) analysis using isolated primary bone marrow-derived macrophage cells from the marrow (Figure 4*D*–*F*). The SCAP$^{\Delta M\varphi}$ mice and the SCAP$^{fl/fl}$ control mice were subjected to a 12-week PD-feeding protocol to observe improvement in steatohepatitis and a 16-week PD-feeding protocol to observe improvement in liver fibrosis (Figure 4*G*).

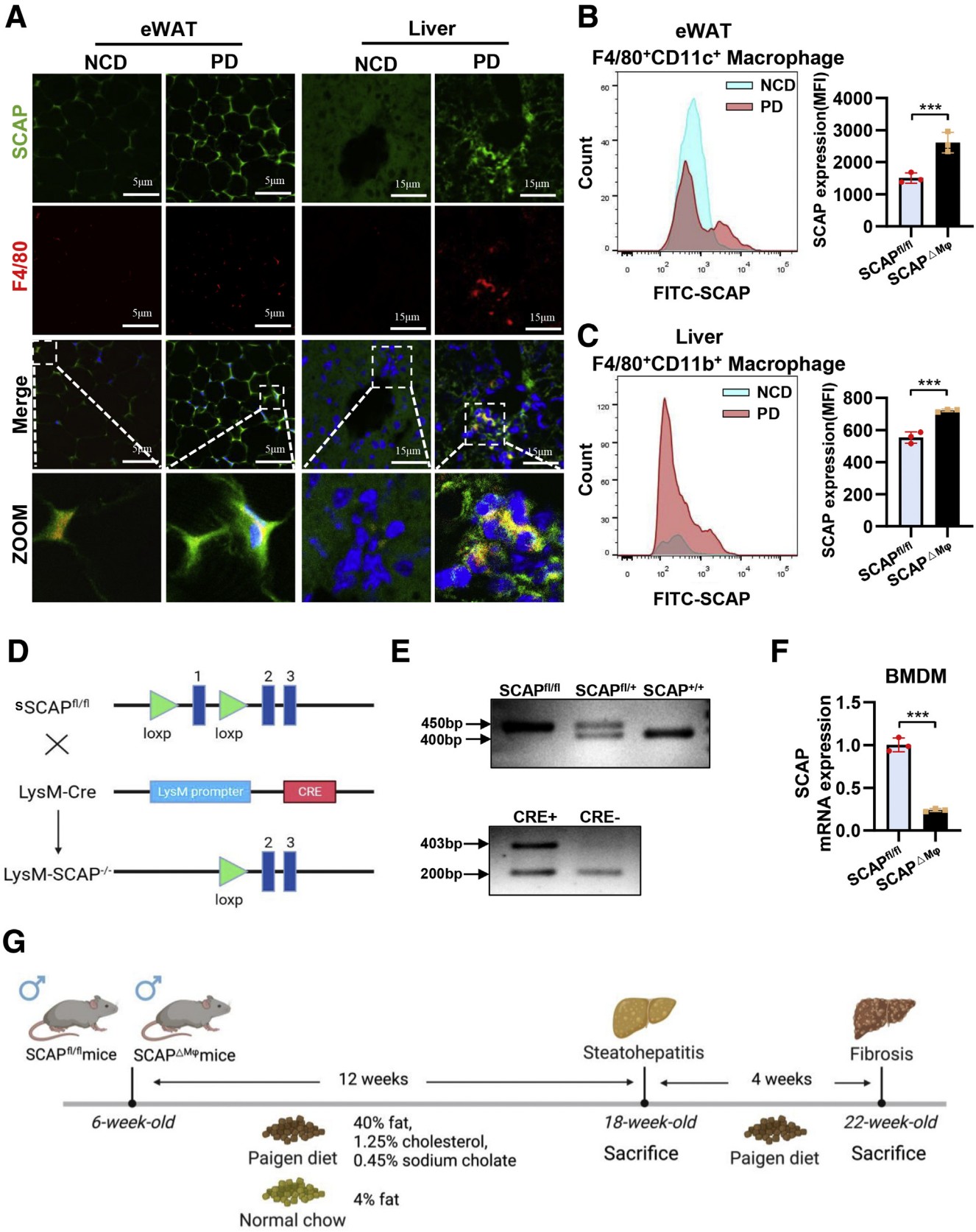


**Figure 4. Macrophage SCAP expression is abnormally increased in eWAT and liver tissues of PD-fed mice.** (*A*) Immunofluorescence staining of SCAP and F4/80 in eWAT and liver tissues (n = 3). (*B*) Flow cytometry was used to analyze expression of SCAP in F4/80$^{+}$CD11c$^{+}$ macrophages of eWAT (n = 3). (*C*) Flow cytometry was used to analyze expression of SCAP in F4/80$^{+}$CD11b$^{+}$ macrophages of liver tissues (n = 3). (*D*) Mice with macrophage/monocyte-specific deletion of SCAP (SCAP$^{\Delta M\varphi}$ mice) were generated by crossing SCAP$^{fl/fl}$ mice with LysM Cre mice. (*E*) Genotyping SCAP knockout mice by PCR showed different genotypes: SCAP+/+, SCAP+/−, SCAP−/−. (*F*) Relative mRNA levels of SCAP in bone marrow-derived macrophage cells. (*G*) Schematic outline of experimental approaches and analyses. Data are expressed as mean ± SD. *$P$ < .05; **$P$ < .01; ***$P$ < .0001; ns, nonsignificant (2-tailed unpaired $t$ test in bar graphs).

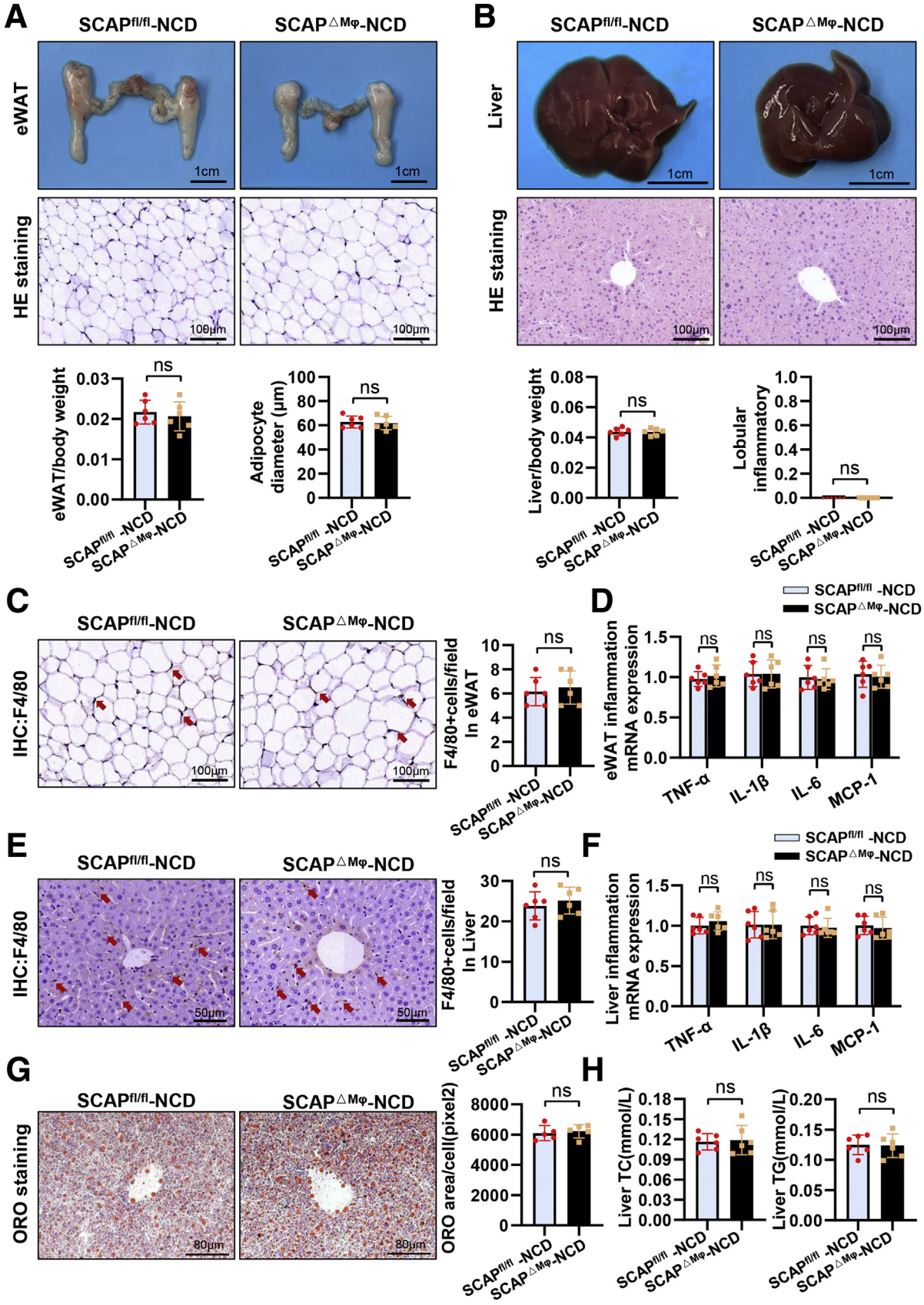


**Figure 5. Macrophage SCAP deletion does not alter eWAT and liver phenotype in NCD-fed mice.** (*A*) Representative pictures and H&E staining of eWAT, and the histogram represents eWAT/body weight (n = 6). (*B*) Representative pictures and H&E staining of liver tissues, and the histogram represents liver/body weight (n = 6). (*C*) Immunohistochemical staining of F4/80$^+$ cells in eWAT (n = 6). (*D*) Relative mRNA levels of IL1$\beta$, IL6, TNF-$\alpha$, and MCP-1 in eWAT (n = 6). (*E*) Immunohistochemical staining of F4/80$^+$ cells in liver tissues (n = 6). (*F*) Relative mRNA levels of IL1$\beta$, IL6, TNF-$\alpha$, and MCP-1 in liver tissues (n = 6). (*G*) Representative images of Oil Red O staining in liver tissues (n = 6). (*H*) Levels of intrahepatic TC and TG (n = 6). Data are expressed as mean ± SD. *$P < .05$; **$P < .01$; ***$P < .0001$; ns, nonsignificant (2-tailed unpaired *t* test in bar graphs).

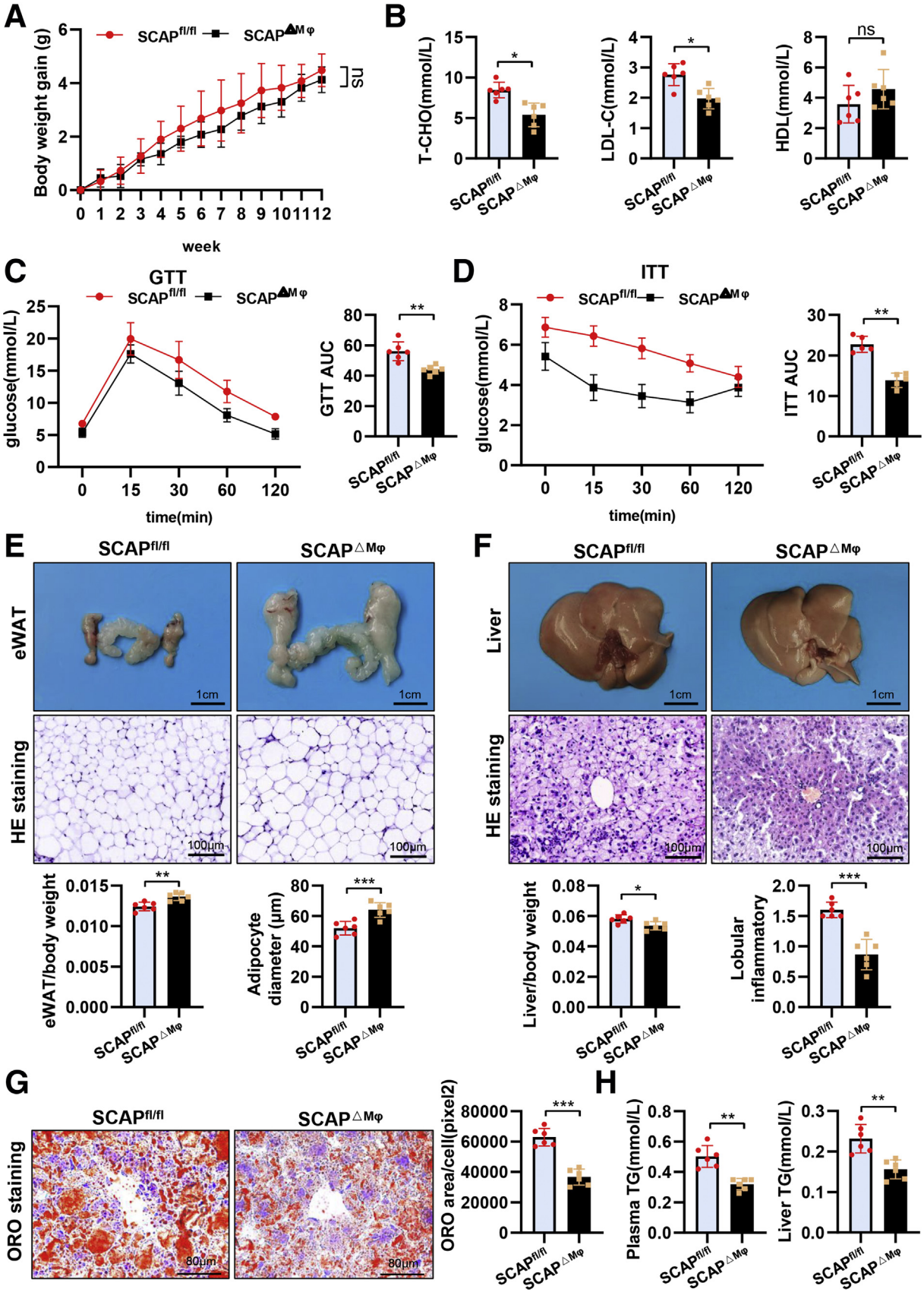


**Figure 6. Macrophage SCAP deletion improves metabolic syndrome and lean NAFLD in PD-fed mice.** (*A*) Body weight gain curves of SCAP$^{fl/fl}$ and SCAP$^{\Delta M\varphi}$ mice fed 12 weeks of PD (n = 6). (*B*) Levels of TC, HDL, and LDL in plasma (n = 6). GTT levels (*C*) and ITT levels (*D*) in SCAP$^{\Delta M\varphi}$ and SCAP$^{fl/fl}$ mice (n = 6). (*E*) Representative pictures and H&E staining of eWAT, and the histogram represents eWAT/body weight (n = 6). (*F*) Representative pictures and H&E staining of liver tissues, and the histogram represents liver/body weight (n = 6). (*G*) Representative images of Oil Red O staining in liver tissues (n = 6). (*H*) Levels of TG in plasma and intrahepatic TG levels (n = 6). Data are expressed as mean ± SD. $^{*}P < .05$; $^{**}P < .01$; $^{***}P < .0001$; ns, nonsignificant (2-tailed unpaired *t* test in bar graphs and two-way analysis of variance in body weight, GTT, and ITT curves).

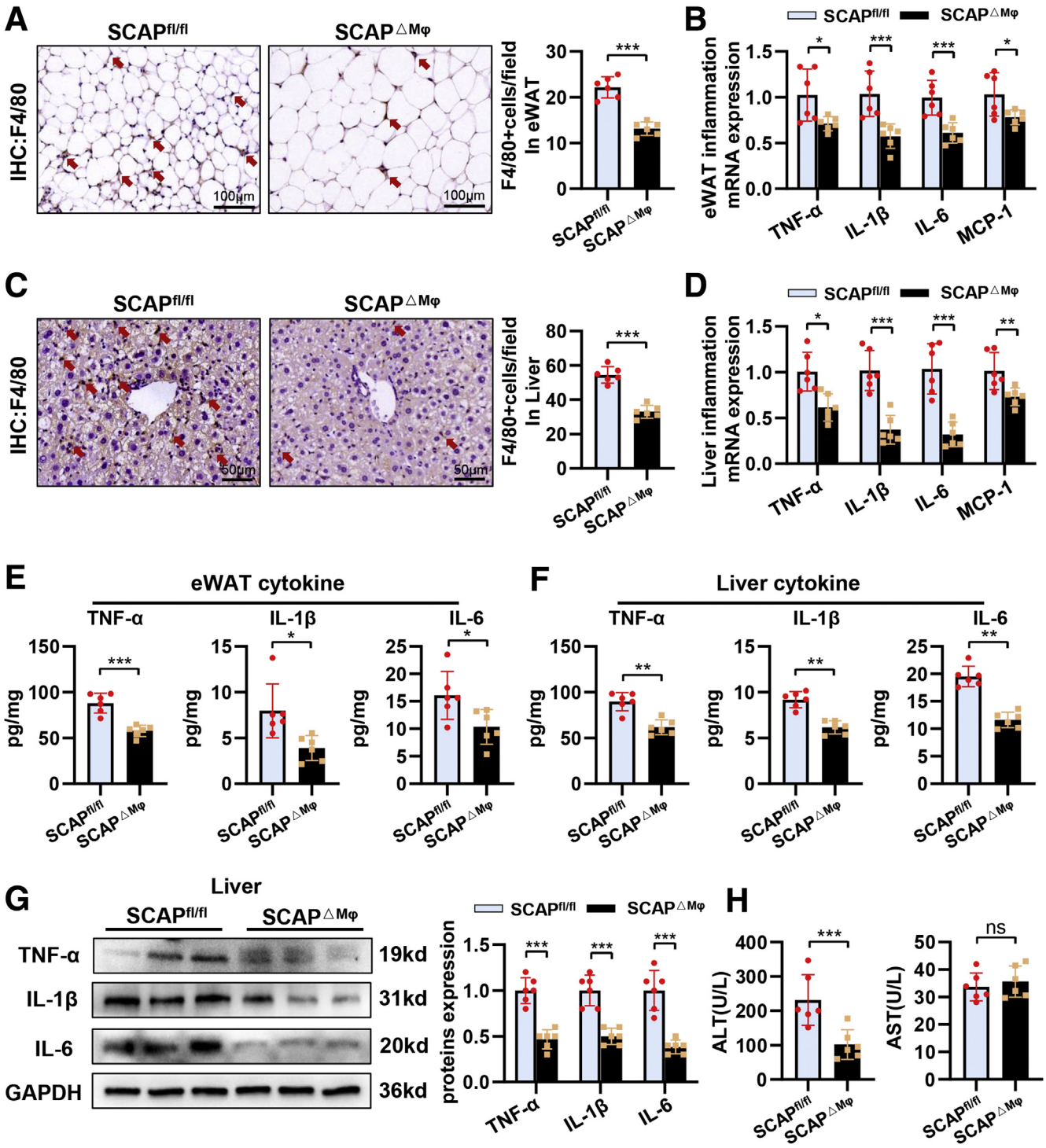


**Figure 7. Macrophage SCAP deletion has ameliorative effects on metaflammation in eWAT and liver tissue of PD-fed mice.** (*A*) Immunohistochemical staining of F4/80$^+$ cells in eWAT (n = 6). (*B*) Relative mRNA levels of IL1$\beta$, IL6, TNF-$\alpha$, and MCP-1 in eWAT (n = 6). (*C*) Immunohistochemical staining of F4/80$^+$ cells in liver tissues (n = 6). (*D*) Relative mRNA levels of IL1$\beta$, IL6, TNF-$\alpha$, and MCP-1 in liver tissues (n = 6). Enzyme-linked immunosorbent assay analysis of protein expression of IL1$\beta$, IL6, and TNF-$\alpha$ in eWAT (*E*) and in liver tissues (*F*) (n = 6). (*G*) Protein levels of TNF-$\alpha$, IL1$\beta$, and IL6 in liver tissues (n = 6). (*H*) Levels of ALT and aspartate aminotransferase in plasma (n = 6). Data are expressed as mean ± SD. **P* < .05; ***P* < .01; ****P* < .0001; ns, nonsignificant (2-tailed unpaired *t* test in bar graphs).

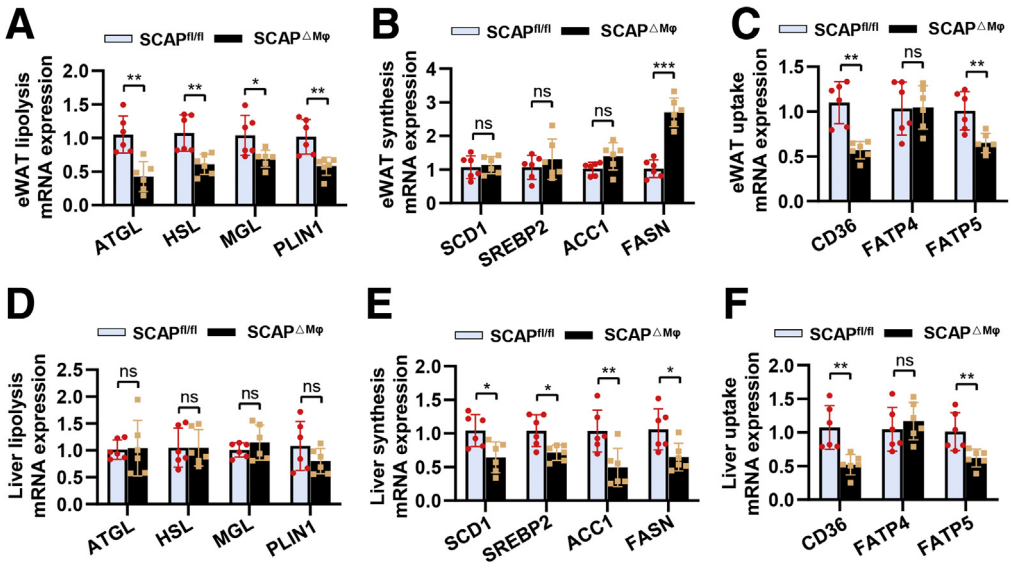


**Figure 8. Macrophage SCAP deletion has ameliorative effects on lipid disorders in eWAT and liver tissue of PD-fed mice.** Relative mRNA levels of lipolysis (*A*), lipid synthesis (*B*), and lipid uptake (*C*) in eWAT (n = 6). Relative mRNA levels of lipolysis (*D*), lipid synthesis (*E*), and lipid uptake (*F*) in liver tissues (n = 6). Data are expressed as mean ± SD. $^{*}P < .05$; $^{**}P < .01$; $^{***}P < .0001$; ns, nonsignificant (2-tailed unpaired *t* test in bar graphs).

## Macrophage SCAP Deletion Improves Metabolic Syndrome and Lean NAFLD in PD-Fed Mice

First, we checked the effect of macrophage-specific SCAP knockout on the lipid homeostasis and inflammation in eWAT and liver; the results indicate that there were no differences in eWAT and liver tissue weight, pathology, inflammation, and lipid content of $SCAP^{\Delta M\varphi}$ mice and $SCAP^{fl/fl}$ mice under NCD-feeding condition (Figure 5). Then, we observed that metabolism-related indicators, hyperlipidemia, impaired glucose tolerance, and insulin sensitivity were significantly ameliorated in $SCAP^{\Delta M\varphi}$ mice of 12 weeks PD-fed, although the weight loss was not reversed (Figure 6*A*–*D*). The weight of eWAT and the size of adipocytes were increased in PD-fed $SCAP^{\Delta M\varphi}$ mice (Figure 6*E*). Liver weight, hepatocyte lobular inflammatory infiltration, lipid accumulation, plasma TG, and intrahepatic levels were reduced in $SCAP^{\Delta M\varphi}$ mice compared with $SCAP^{fl/fl}$ control mice (Figure 6*F*–*H*). These findings suggest that macrophage-specific deficiency of SCAP can improve metabolic syndrome and lean NAFLD in PD-fed mice.

## Macrophage SCAP Deletion Has Ameliorative Effects on Lipid Disorders and Metaflammation in the eWAT and Liver Tissue of PD-Fed Mice

Furthermore, we observed that the macrophages infiltration and expression of proinflammatory cytokines (IL1$\beta$, IL6, TNF-$\alpha$, and MCP-1) were reduced in eWAT and liver tissues of $SCAP^{\Delta M\varphi}$ mice (Figure 7*A*–*G*). Plasma ALT level was reduced (Figure 7*H*). We detected lipid uptake, synthesis, and lipolysis in eWAT and liver tissues of $SCAP^{\Delta M\varphi}$ mice. In eWAT, lipolysis gene mRNA (ATGL, HSL, MGL, PLIN1) and the lipid uptake gene mRNA (CD36 and FATP5) were clearly reduced, whereas the lipid synthesis gene mRNA (FASN) was increased in PD-fed $SCAP^{\Delta M\varphi}$ mice (Figure 8*A*–*C*), indicating that the lipid storage function of adipocytes was restored. In the liver, the lipid uptake gene mRNA (CD36 and FATP5) and the lipid synthesis gene mRNA (SCD1, SREBP2, ACC1, and FASN) expression levels were reversed because of macrophage SCAP deletion but had no effect on the lipolysis gene mRNA (ATGL, HSL, MGL, and PLIN1) expression (Figure 8*D*–*F*). All these data suggest that SCAP deletion in macrophages could reverse lipid disorders and metaflammation in the eWAT and liver tissue of PD-fed mice.

## Expression Levels of SCAP in Macrophages Also Influence Lipid Homeostasis and Inflammatory Response of Adipocytes/Hepatocytes in Vitro

Next, we attempted to identify macrophage SCAP could regulate the lipid metabolism process in vitro using the macrophage-adipocytes/hepatocytes cell coculture system. We cocultured overexpression or knockdown of SCAP in RAW264.7 macrophage cells with 3T3-L1 adipocyte cells in low-density lipoprotein (LDL) cholesterol loading medium (Figure 9*A*). RAW264.7 cells SCAP overexpression reduced the lipid accumulation in 3T3-L1 cells by promoting inflammatory response and up-regulating lipolysis and down-regulating lipid synthesis, although the lipid uptake was modestly increased (Figure 9*B*–*F*). These results were further supported in SCAPi RAW264.7 cells, which increased lipid accumulation by reducing inflammatory response, lipolysis, and lipid uptake, while promoting lipid synthesis in 3T3-L1 cells due to SCAP knockdown (Figure 9*G*–*K*).

The same observations were done by using the THP-1/HepG2 cell coculture system (Figure 10*A*). SCAP overexpression in THP-1 cells increased HepG2 cells lipid content, proinflammatory cytokines, lipid uptake, synthesis, and lipolysis (Figure 10*B*–*F*). Conversely, SCAP knockdown in THP-1 cells reduced HepG2 cells lipid content, proinflammatory cytokines, lipid uptake, lipid synthesis, and lipolysis (Figure 10*G*–*K*). These in vitro data support the in vivo observations and further indicate that macrophage SCAP regulates lipid homeostasis and the inflammatory response in adipocytes and hepatocytes.

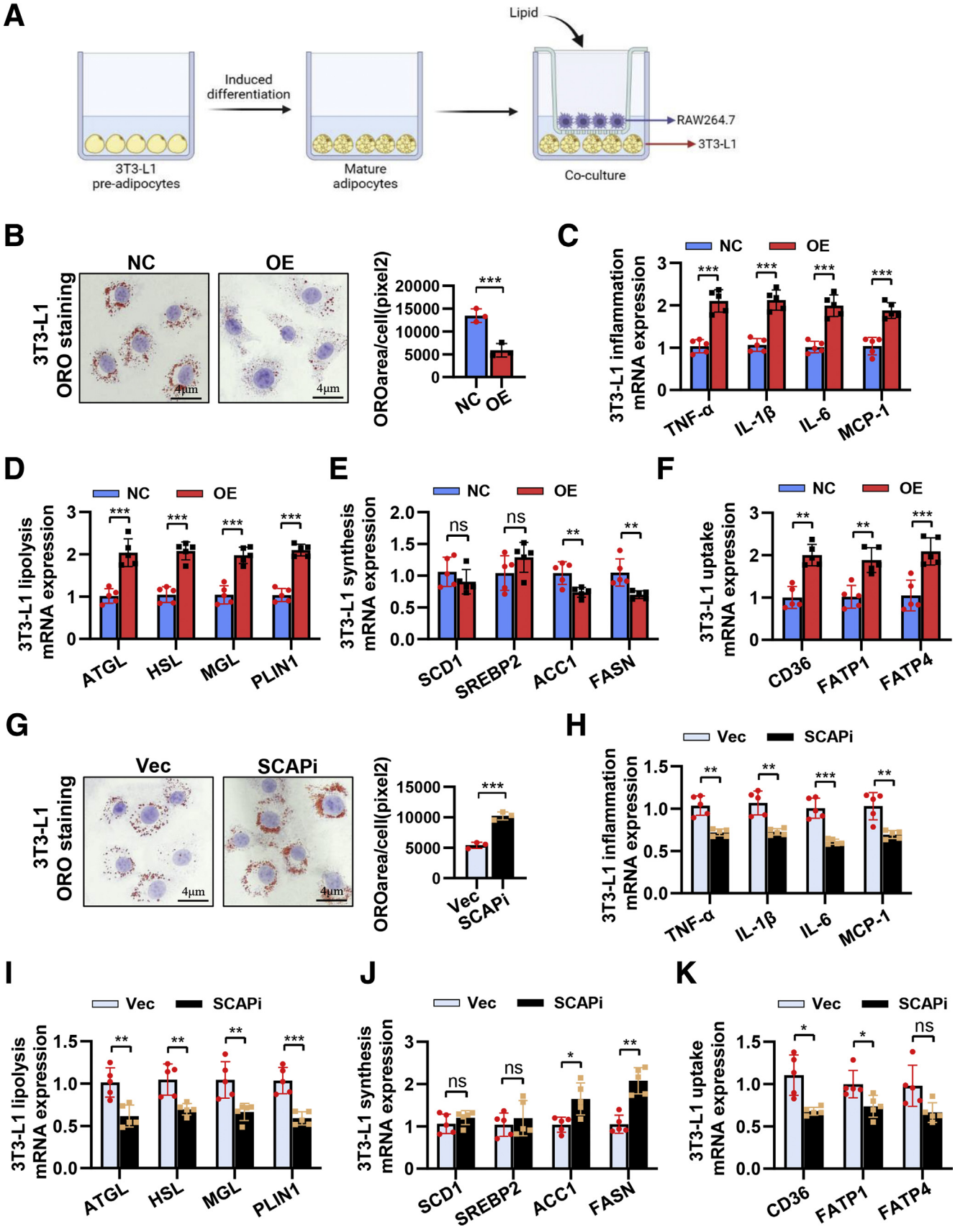
A
Lipid
Induced differentiation
RAW264.7
3T3-L1
3T3-L1 pre-adipocytes
Mature adipocytes
Co-culture
B
NC
OE
3T3-L1 ORO staining
4μm
OROarea/cell(pixel2)
C
3T3-L1 inflammation mRNA expression
TNF-α
IL-1β
IL-6
MCP-1
D
3T3-L1 lipolysis mRNA expression
ATGL
HSL
MGL
PLIN1
E
3T3-L1 synthesis mRNA expression
SCD1
SREBP2
ACC1
FASN
F
3T3-L1 uptake mRNA expression
CD36
FATP1
FATP4
G
Vec
SCAPi
H
I
J
K

## Macrophage SCAP Deletion Alleviates the Inflammatory Response in the eWAT and Liver Tissue of PD-Fed Mice via Inhibition of STING–NF-κB Signaling

To further explore the mechanisms of macrophage SCAP-induced metaflammation, we examined NF-κB inflammatory signaling pathway. First, we quantified the levels of p65 activation (phosphor-p65 and nuclear localization of p65) and found the levels of p65 phosphorylation and P65 nuclear translocation were increased in the liver of PD-fed mice, whereas they were reversed by macrophage SCAP deletion (Figure 11*A*). Activated IκB kinase (IKK) complex induces phosphorylation and degradation of IκBα and subsequent activation of p65 and translocation of p65 into the nucleus.[27] We next examined the activation status of IKK. The data showed that IKK complex (IKKα and IKKβ) was phosphorylated and targeted IκBα (phosphor- IκBα) for degradation, but SCAP deletion inhibited this process (Figure 11*B*). We further determined that the liver and eWAT inflammation resulted from the p65 nuclear translocation in macrophage by immunofluorescence microscopy using macrophage-specific probe F4/80 and anti-P65 (Figure 11*C*).

STING/TBK1 is a classical innate immune signaling pathway, and recent evidence suggests that STING/TBK1 is important for the inflammatory response in metabolic diseases by activating NF-κB (Figure 11*D*).[28,29] We observed elevated expression of STING and P-TBK1 in liver of PD-fed mice, which depended on the presence of SCAP (Figure 11*E*). Because STING is expressed specifically in macrophages (Figure 11*F* and *G*),[30] the increased STING expression in liver tissue is associated with the presence of macrophage infiltration. These results were not significantly different in NCD-fed $SCAP^{\Delta M\varphi}$ mice and $SCAP^{fl/fl}$ mice (Figure 12). Similar results were found in eWAT (Figure 13). These data suggest that p65 activation results from the activities of STING/TBK1 signal and thus activates the inflammatory response in the liver and eWAT of PD-fed mice. This process can be blocked by macrophage SCAP deletion.

## SCAP Promotes Inflammatory Response Through STING–NF-κB Signaling Activation in Vitro

Moreover, we also validated the effect of SCAP on the STING–NF-κB signaling pathway in vitro. We overexpressed or knocked down the SCAP in RAW264.7 murine macrophage cells. The gene expression of inflammatory cytokines was lower in SCAPi-RAW264.7 cells than in Vec-RAW264.7 cells. Conversely, the expression of inflammatory cytokines was increased by SCAP overexpressed treatment (Figure 14*A* and *B*). We demonstrated that P-p65 expression was increased in OE-SCAP-RAW264.7 cells but reduced in SCAPi-RAW264.7 cells (Figure 14*C*). We observed enhanced nuclear translocation of P65 in OE-SCAP-RAW264.7 cells but decreased translocation in SCAPi-RAW264.7 cells (Figure 14*D*–*F*). Meanwhile, we verified the expression of STING–NF-κB signaling pathway. The data showed that SCAP overexpression could not change STING expression but strongly stimulated the phosphorylation TBK1–NF-κB, whereas knockdown of SCAP resulted in the opposite effect (Figure 14*G*). These data suggest that SCAP activates the STING–NF-κB signaling pathway in macrophages to stimulate the inflammatory response.

## SCAP Recruits STING and TBK1 to the Golgi and Activates NF-κB Signaling

STING recruits and phosphorylates TBK1 on the Golgi[31,32] and then phosphorylates IKK to initiate transcription of NF-κB.[33] Because SCAP and STING/TBK1 similarly play biological roles in the Golgi, we observed a correlation between the SCAP and STING/TBK1 (Figure 15*A*). We tested whether SCAP might directly interact with STING and TBK1. Immunofluorescence confirmed the co-localization of SCAP with STING in liver and RAW264.7 cells (Figure 15*B* and *C*). Co-immunoprecipitation (Co-IP) experiments showed that SCAP interacted intensely with STING but not with TBK1 (Figure 15*D*). We confirmed that knockdown of SCAP dramatically reduced STING and TBK1 colocalization with the Golgi in RAW264.7 cells via confocal microscopy (Figure 15*E*). Meanwhile, blocking SCAP translocation on the Golgi by 25-hydroxycholesterol (25-HC), a SCAP translocation inhibitor from the ER to the Golgi,[20] inhibited the colocalization of STING and TBK1 with the Golgi, although in the presence of SCAP overexpression (Figure 15*F*). Consistently, we found that P65 nuclear translocation and the STING–NF-κB signaling pathway were inhibited by 25-HC treatment in overexpression of SCAP–RAW264.7 cells (Figure 15*G* and *H*). Taken together, these data indicate that the location of SCAP on the Golgi is required for activation of the STING–NF-κB signaling pathway.

## Macrophage SCAP Deletion Ameliorates the Degree of Liver Fibrosis in PD-Fed Mice

The prognosis of NAFLD closely correlates with the degree of liver fibrosis, which is the most important clinical challenge in NAFLD. The patients with lean NAFLD have a faster fibrosis progression, compared with the obese NAFLD

**Figure 9.** (***See previous page***). **Expression levels of SCAP in macrophages also influences lipid homeostasis and inflammatory response of adipocytes in vitro.** (*A*) Schematic diagram of cocultivation of 3T3-L1 cells and RAW264.7 cells. (*B*) Oil Red O staining of LDL-treated 3T3-L1 cells cocultured with NC-SCAP or OE-SCAP RAW264.7 cells (n = 3). Relative mRNA levels of inflammation cytokine (*C*), lipolysis (*D*), lipid synthesis (*E*), and lipid uptake (*F*) in LDL-treated 3T3-L1 cells cocultured with NC-SCAP or OE-SCAP RAW264.7 cells (n = 5). (*G*) Oil Red O staining of LDL-treated 3T3-L1 cells cocultured with Vec-SCAP or SCAPi-RAW264.7 cells (n = 3). Relative mRNA levels of inflammation cytokine (*H*), lipolysis (*I*), lipid synthesis (*J*), and lipid uptake (*K*) in LDL-treated 3T3-L1 cells cocultured with Vec-SCAP or SCAPi-RAW264.7 cells (n = 5). Data are expressed as mean ± SD. **P* < .05; ***P* < .01; ****P* < .0001; ns, nonsignificant (2-tailed unpaired *t* test in bar graphs).

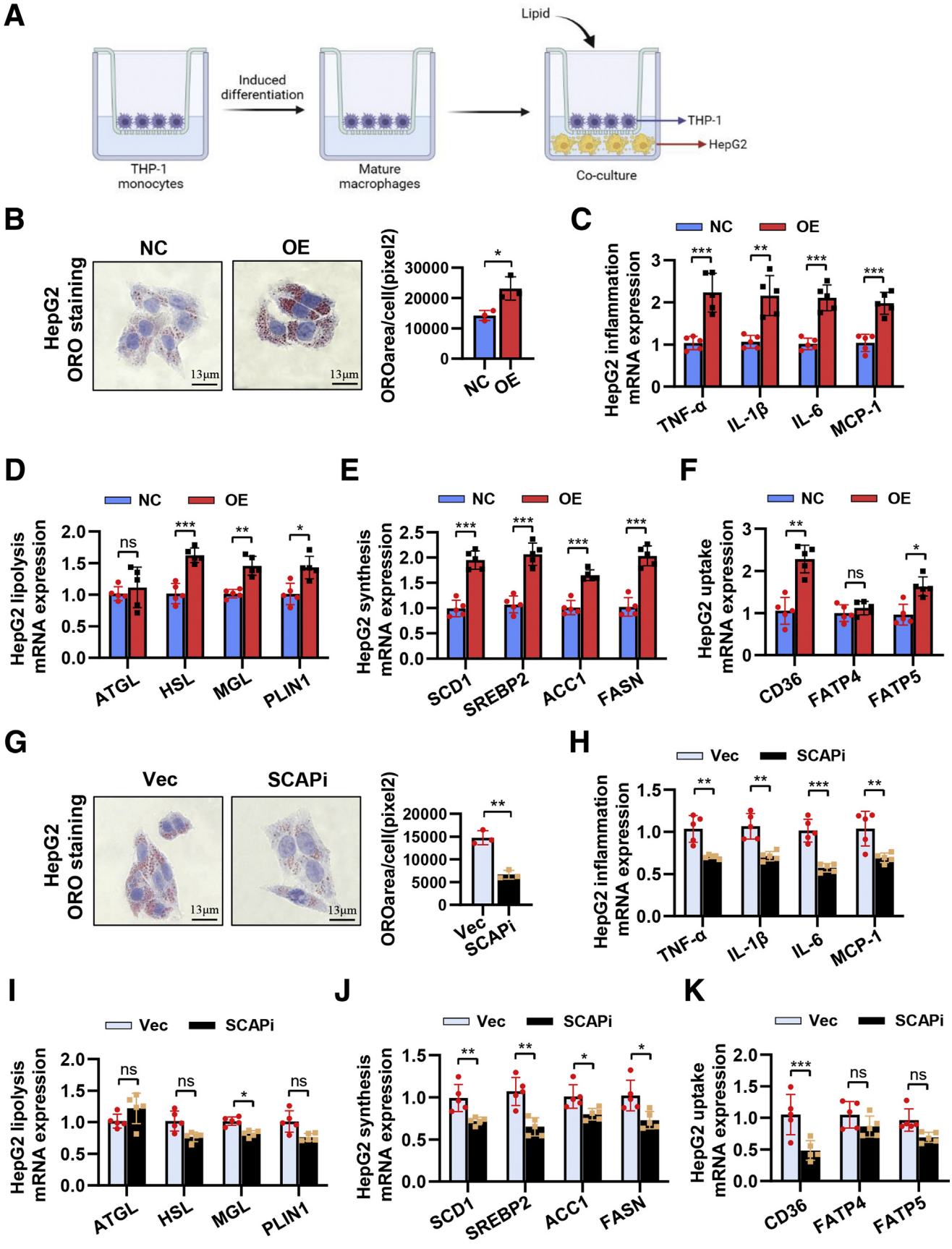
A
Lipid
Induced differentiation
THP-1
HepG2
THP-1 monocytes
Mature macrophages
Co-culture
B
NC
OE
HepG2 ORO staining
13μm
OROarea/cell(pixel2)
C
HepG2 inflammation mRNA expression
TNF-α
IL-1β
IL-6
MCP-1
D
HepG2 lipolysis mRNA expression
ATGL
HSL
MGL
PLIN1
E
HepG2 synthesis mRNA expression
SCD1
SREBP2
ACC1
FASN
F
HepG2 uptake mRNA expression
CD36
FATP4
FATP5
G
Vec
SCAPi
H
I
J
K

patients. We further examined the effects of SCAP deletion on a 16-week PD-feeding protocol induced steatohepatitis and liver fibrosis. After PD feeding for 16 weeks, hepatocyte steatosis, lobular inflammatory infiltration, macrophage infiltration, fibrosis, and plasma levels of ALT in $SCAP^{\Delta M\varphi}$ mice were significantly ameliorated, compared with control $SCAP^{fl/fl}$ mice (Figure 16*A*–*C*). Consistently, the degree of fibrosis and proinflammatory cytokines in $SCAP^{\Delta M\varphi}$ mice was significantly lighter than in $SCAP^{fl/fl}$ mice (Figure 16*D*–*F*). Meanwhile, the STING expression, phosphorylated TBK1 and p65 levels were lower in $SCAP^{\Delta M\varphi}$ mice than in $SCAP^{fl/fl}$ mice (Figure 16*G*). These results suggest that macrophage SCAP deficiency ameliorates liver fibrosis and reduces the hepatic STING–NF-κB signaling pathway activation.

## Discussion

SCAP is recognized as an important regulator of cholesterol metabolism. In the current study, we provide novel evidence that abnormally increased macrophage SCAP plays a critical role in the development of metaflammation during lean NAFLD progression. We confirmed that macrophage SCAP-specific knockout significantly ameliorates PD-induced hyperlipidemia, insulin resistance, and lean NAFLD by reducing tissue inflammation. The mechanism is that macrophage SCAP-specific knockout improved local inflammation in the liver and adipose tissue by attenuating STING–NF-kB signaling pathway activation. Our findings provide new mechanistic insight into the pathogenesis of lean NAFLD.

Various diets, including PD, high-fat diet, and methionine-choline deficient, could induce a mouse NAFLD model; therefore, they are used to study the pathogenesis and treatment of NAFLD. Interestingly, PD-induced NAFLD was accompanied by weight loss, which closely resembled the model of lean NAFLD. Compared with the other feeds, PD contains higher cholesterol, which leads to intestinal flora disorders and severe tissue inflammation.[18,34] In this study, we successfully applied PD to construct a lean NAFLD model accompanied by severe metaflammation. Meanwhile, we observed an overt inflammatory response in eWAT and liver tissues of PD-fed mice that was mediated by macrophage infiltration, resulting in separate phenotypes of lipid metabolism disorder and increasing the influx of lipids from adipose tissue to the liver. These data indicated that cholesterol seems to be more lipotoxic than TG and may be a trigger for the progression of lean NAFLD.

Compared with obese NAFLD, lean NAFLD is mainly characterized by a decrease in subcutaneous adipose tissue. Adipose tissue is a critical lipid storage and release site, where lipids are primarily stored as TG in adipocytes.[35] However, when the limit for storage of lipids is reached or adipocyte lipolysis is dysregulated, lipids can accumulate in ectopic tissues such as the liver, leading to insulin insensitivity and NAFLD.[36] Lipodystrophy is associated with an inflammatory environment, especially inflammatory factors released by activated macrophages, which stimulate lipolysis by increasing the expression of lipolysis-related enzymes and activating the JAK/STAT pathway.[37,38] Our study also confirmed that massive macrophage infiltration in adipose tissue leads to severe inflammation, resulting in adipose tissue lipolysis and increased lipid uptake and synthesis by the liver, which is the main cause of ectopic lipid deposition in PD-fed mice.

Like adipose tissue, there are substantial macrophage infiltration and clear inflammation in the liver. Interestingly, this severe inflammatory response leads to the uptake of lipids from circulating blood and increased lipid synthesis within the liver. Inflammation mediates the heterogeneity of lipid metabolism in eWAT, and liver tissue may be a potential mechanism for the development of lean NAFLD. The activation of hepatic macrophages and subsequent secretion of proinflammatory mediators lead to increased lipid accumulation and damage in hepatocytes, which are critical events in the development and progression of NAFLD.[39,40] PD causes macrophage infiltration and abnormal SCAP expression in macrophages, producing a severe inflammatory response. Therefore, metabolic disturbances manifest as increased adipose tissue lipolysis, and increased accumulation in the liver tissue mediated by inflammation is central to ectopic lipid deposition.

High levels of metaflammation have a major impact on the development of lean NAFLD, forcing us to explore the origins of metaflammation mediated by a high cholesterol diet. As a cholesterol sensitizer, SCAP has been of interest to us as a key bridging molecule between metabolism and inflammation. Cholesterol homeostasis disorder and the large amount of lipopolysaccharide (LPS) that originated from the intestine caused by PD stimulated an abnormal increase in macrophage SCAP, which further had an amplifying effect on the production of inflammatory factors. SCAP has been shown to play a key role in metabolic diseases through the regulation of inflammatory signaling pathways such as NLRP3 and NF-κB.[24–26] In this study, we found that the macrophage NF-κB signaling pathway was significantly activated in PD-fed mice but rescued in $SCAP^{\Delta M\varphi}$ mice. Therefore, we determined that the modulatory effect of SCAP on the NF-κB signaling pathway is an important mechanism for triggering metaflammation in PD-fed mice.

**Figure 10.** (***See previous page***). **Expression levels of SCAP in macrophages also influences lipid homeostasis and inflammatory response of adipocytes in vitro.** (*A*) Schematic diagram of cocultivation of HepG2 cells and THP-1 cells. (*B*) Oil Red O staining of LDL-treated HepG2 cells cocultured with NC-SCAP or OE-SCAP THP-1 cells (n = 3). Relative mRNA levels of inflammation cytokine (*C*), lipolysis (*D*), lipid synthesis (*E*), and lipid uptake (*F*) in LDL-treated HepG2 cells cocultured with NC-SCAP or OE-SCAP THP-1 cells (n = 5). (*G*) Oil Red O staining of LDL-treated HepG2 cells cocultured with Vec-SCAP or SCAPi-THP-1 cells (n = 3). Relative mRNA levels of inflammation cytokine (*H*), lipolysis (*I*), lipid synthesis (*J*), and lipid uptake (*K*) in LDL-treated HepG2 cells cocultured with Vec-SCAP or SCAPi-THP-1 cells (n = 5). Data are expressed as mean ± SD. $^{*}P < .05$; $^{**}P < .01$; $^{***}P < .0001$; ns, nonsignificant (2-tailed unpaired *t* test in bar graphs).

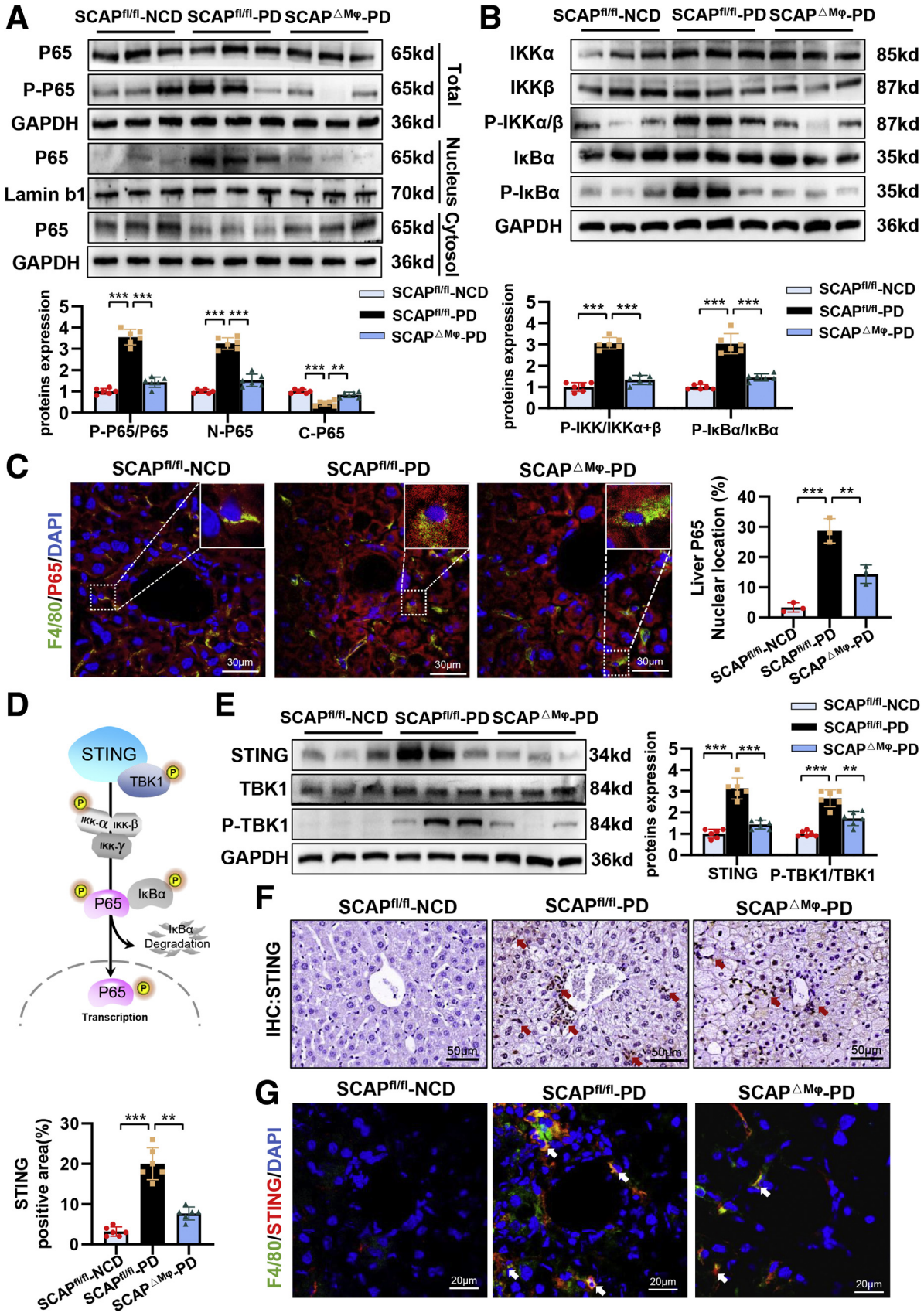


**Figure 11. Macrophage SCAP deletion alleviates inflammatory response in liver tissue of PD-fed mice via inhibition of STING–NF-κB signaling.** (*A*) Protein levels of P65 and P-P65 in total liver tissues, P65 in liver nuclear and cytosol (n = 6). (*B*) Protein levels of IKK$\alpha$, IKK$\beta$, P-IKK$\alpha/\beta$, I$\kappa$B$\alpha$, and P-I$\kappa$B$\alpha$ in liver tissues (n = 6). (*C*) Immunofluorescence staining of F4/80 and P65 in liver tissues (n = 3). (*D*) Schematic diagram of mechanisms by which STING activates NF-$\kappa$B signaling. (*E*) Protein levels of STING, P-TBK1, and TBK1 in liver tissues (n = 6). (*F*) Immunohistochemical staining of STING in liver tissues (n = 6). (*G*) Immunofluorescence staining of F4/80 and STING in liver tissues (n = 3). Data are expressed as mean ± SD. **P* < .05; ***P* < .01; ****P* < .0001; ns, nonsignificant (2-tailed unpaired *t* test in bar graphs).

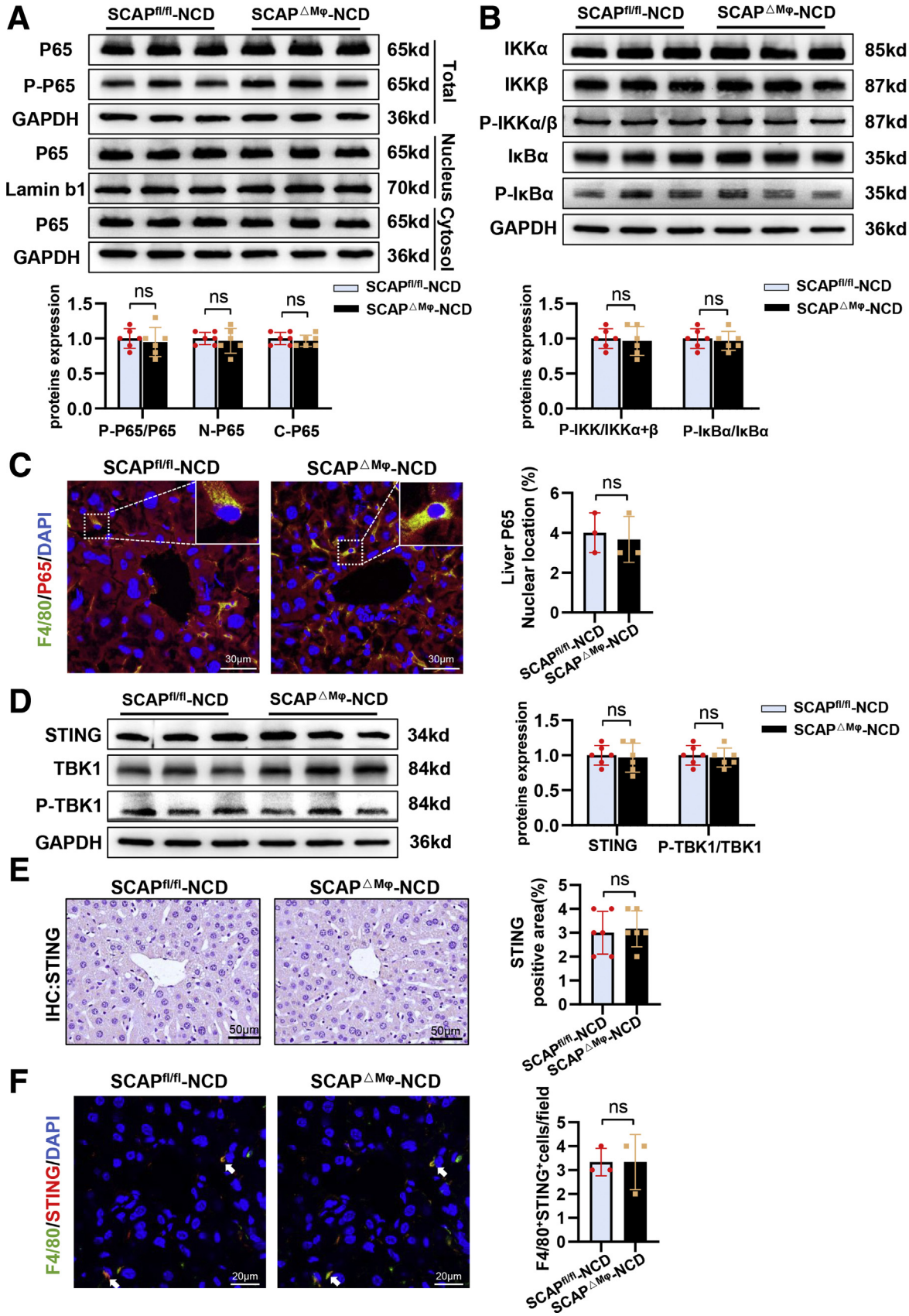


**Figure 12. Macrophage SCAP deletion does not alter STING–NF-κB signaling in liver tissue of NCD-fed mice.** (*A*) Protein levels of P65 and P-P65 in total liver tissues, P65 in liver nuclear and cytosol (n = 6). (*B*) Protein levels of IKK$\alpha$, IKK$\beta$, P-IKK$\alpha/\beta$, I$\kappa$B$\alpha$, and P-I$\kappa$B$\alpha$ in liver tissues (n = 6). (*C*) Immunofluorescence staining of F4/80 and P65 in liver tissues (n = 3). (*D*) Protein levels of STING, P-TBK1, and TBK1 in liver tissues (n = 6). (*E*) Immunohistochemical staining of STING in liver tissues (n = 6). (*F*) Immunofluorescence staining of F4/80 and STING in liver tissues (n = 3). Data are expressed as mean ± SD. **P* < .05; ***P* < .01; ****P* < .0001; ns, nonsignificant (2-tailed unpaired *t* test in bar graphs).

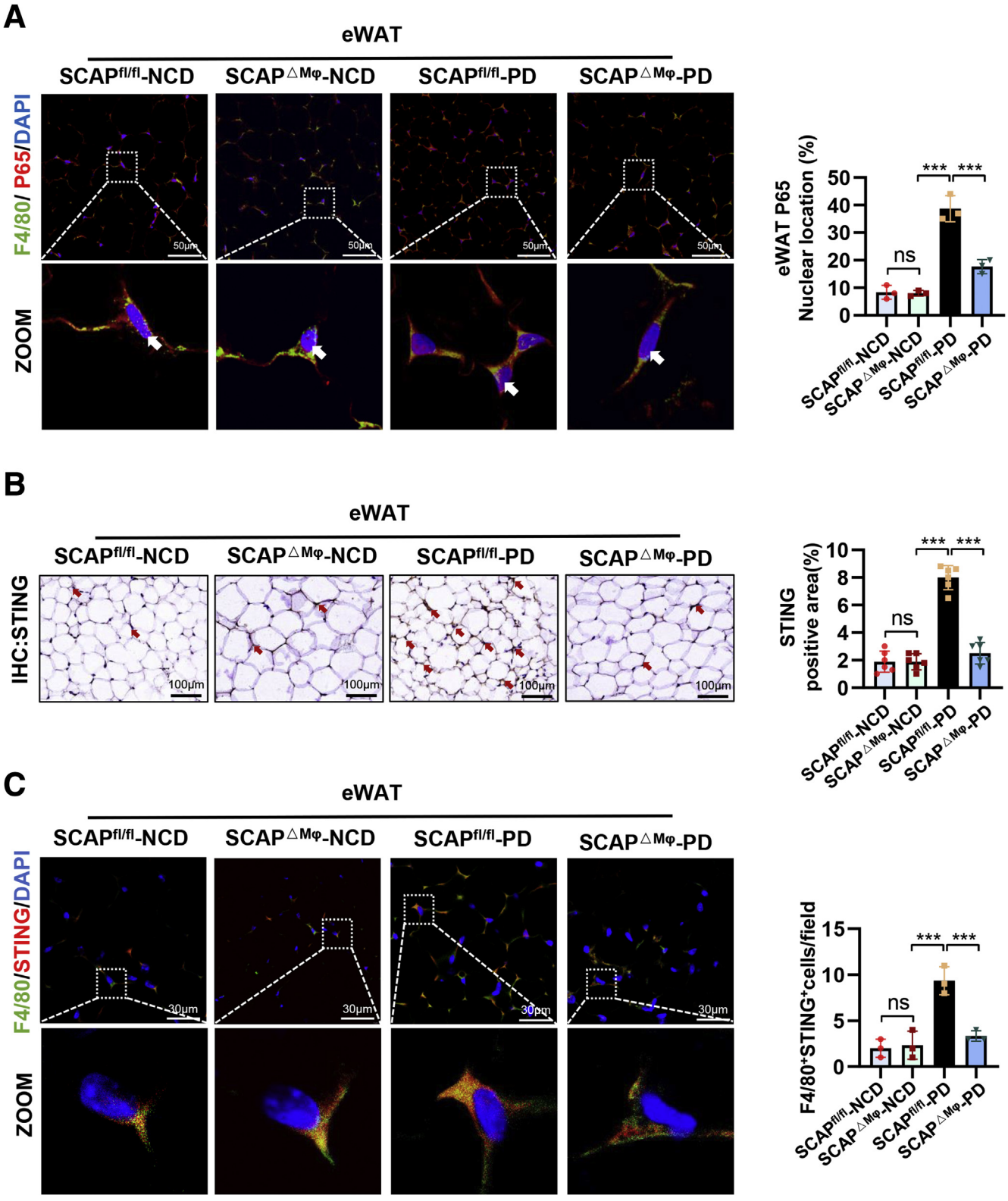


**Figure 13. Macrophage SCAP deficiency inhibits expression of STING and P65 in eWAT of PD-fed mice.** (*A*) Immunofluorescence staining of F4/80 and P65 in eWAT (n = 3). (*B*) Immunohistochemical staining of STING in eWAT (n = 6). (*C*) Immunofluorescence staining of F4/80 and STING in eWAT (n = 3). Data are expressed as mean ± SD. $^{*}P < .05$; $^{**}P < .01$; $^{***}P < .0001$; ns, nonsignificant (2-tailed unpaired *t* test in bar graphs).

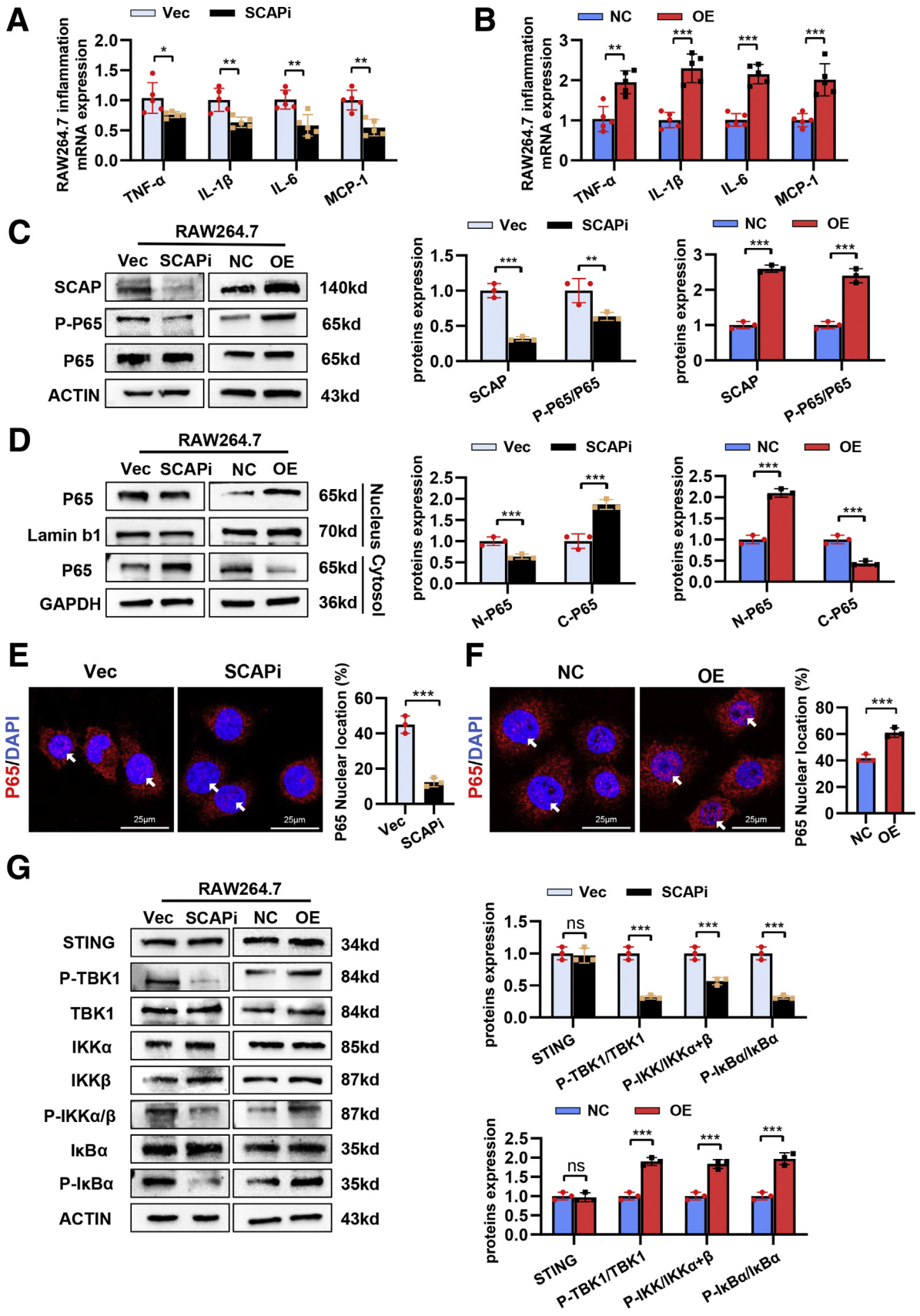
A
Vec
SCAPi
RAW264.7 inflammation mRNA expression
TNF-α
IL-1β
IL-6
MCP-1
B
NC
OE
C
RAW264.7
Vec SCAPi NC OE
SCAP 140kd
P-P65 65kd
P65 65kd
ACTIN 43kd
proteins expression
SCAP
P-P65/P65
D
Nucleus
Cytosol
Lamin b1 70kd
GAPDH 36kd
N-P65
C-P65
E
F
P65/DAPI
25μm
P65 Nuclear location (%)
G
STING 34kd
P-TBK1 84kd
TBK1 84kd
IKKα 85kd
IKKβ 87kd
P-IKKα/β 87kd
IκBα 35kd
P-IκBα 35kd
ACTIN 43kd
ns
STING
P-TBK1/TBK1
P-IKK/IKKα+β
P-IκBα/IκBα

STING plays an important role in infectious diseases by acting as a crucial regulator of the DNA sensing pathway. The STING/TBK1 signaling pathway has been found to be responsible for the development of metabolic disease in recent years[28–30]; however, the mechanism of activation in metaflammation is still unknown. In our work, the intrahepatic STING–NF-κB signaling pathway was significantly activated in PD-induced NAFLD, and this phenotype was rescued in SCAP$^{\Delta M\varphi}$ mice. Previous reports and our data confirm that STING is not present in human and mice hepatocytes but expressed at high abundance in hepatic nonparenchymal cells.[29,30] The decrease of STING expression in SCAP$^{\Delta M\varphi}$ mice may be attributed to the reduction of macrophage infiltration. Inflammation is key to drive NAFLD to nonalcoholic steatohepatitis and fibrosis. In the present study, we verified that SCAP$^{\Delta M\varphi}$ mice can alleviate PD-induced hepatic steatosis and inflammation by inhibiting the STING–NF-κB pathway. The prognosis of NAFLD closely correlates with the degree of liver fibrosis, which is the most important clinical challenge in NAFLD, whereas the lean NAFLD patients have a faster fibrosis progression, compared with the obese NAFLD patients. We also demonstrated that SCAP$^{\Delta M\varphi}$ mice can reduce the extent of liver fibrosis by the same mechanism.

It has been reported that in NAFLD, STING activation markedly increases macrophage proinflammatory status, which in turn increases hepatocyte fat deposition and proinflammatory responses and enhances hepatic stellate cell activation.[29] Mechanistically, LPS can trigger the perinuclear translocation of STING and activate STING in a cytosolic DNA-dependent manner.[31,41] In the lean NAFLD model induced by PD, perinuclear translocation and activation of STING may be mediated by extensive LPS production from intestinal microecological disorders. Upon activation, STING translocates from the ER to the Golgi, where it recruits TBK1 and then activates the NF-κB signaling pathway, driving the release of inflammatory factors.[32,42,43] Coincidentally, the Golgi is also an important platform for the biological function of SCAP, where it is involved in the cleavage activation of SREBPs and the maintenance of cholesterol homeostasis.[26] This suggests the possible interaction of SCAP with STING, and our extensive data provide ample evidence for this possibility. The interaction between SCAP and STING was confirmed by Co-IP and immunofluorescence, and the knockdown of SCAP inhibited the colocalization of STING with the Golgi and suppressed the activation of the TBK1–NF-κB signaling pathway mediated by LPS. Notably, the SCAP translocation inhibitor 25-hydroxycholesterol (25-HC) significantly reduced the localization of STING and TBK1 to the Golgi and inhibited the NF-κB signaling pathway, which provides strong evidence that SCAP contributes to the optimal activation of STING signaling. Our study makes an important addition to the mechanism for the role of STING in metaflammation and provides major theoretical support for subsequent studies.

In conclusion, our findings reveal that abnormally increased macrophage SCAP amplifies the inflammatory response in adipose and liver tissues, leading to metabolic disorders with distinct phenotypes in both tissues, eventually resulting in the development of metabolic syndrome and lean NAFLD. The mechanism involves the inflammatory response after SCAP-mediated activation of the STING–NF-κB signaling pathway in macrophages. Therefore, inhibition of macrophage SCAP may represent a new therapeutic strategy for the treatment of lean NAFLD.

## Materials and Methods

### Animals and Treatments

Macrophage SCAP-specific knockout mice (LysM-Cre SCAP$^{fl/fl}$) were generated by breeding LysM-Cre mice (Shanghai Model Organisms Center, Inc, Shanghai, China) with SCAP$^{fl/fl}$ mice (The Jackson Laboratory, Bar Harbor, ME). Cre-negative SCAP$^{fl/fl}$ littermates were used as controls. Mice were genotyped by PCR; genotyping of SCAP$^{fl/fl}$ mice resulted in a 450 base pair product for the loxP-targeted allele and a 400 base pair product for the wild-type allele. All genotypes were generated on a pure C57BL/6 background.

Male SCAP$^{\Delta M\varphi}$ (LysM-Cre SCAP$^{fl/fl}$) mice and Cre-negative SCAP$^{fl/fl}$ littermates (6–8 weeks of age) were randomly assigned to feeding with NCD (4% fat, D12102C; Research Diets, New Brunswick, NJ) or PD (40% fat, 1.25% cholesterol, 0.45% sodium cholate, D12109C; Research Diets) for 12 weeks (n = 6 per group). All mice were maintained in ventilated cages under controlled conditions of 12-hour light/dark cycles at 22°C and ad libitum feeding. The animals were euthanized under deep anesthesia by intraperitoneal injection with an overdose of pentobarbital sodium (200 mg/kg) to obtain their samples. All experimental protocols adhered to the Guide for the Care and Use of Laboratory Animals published by the U.S. National Institutes of Health (National Research Council, 8th Edition, 2011). All animal studies were approved by the Animal Ethics Committee of Chongqing Medical University.

### Cell Culture and Adipocyte Differentiation

Mouse Raw264.7 macrophages and human THP1 monocytes were cultured in RMPI-1640 medium

**Figure 14. (*See previous page*). SCAP promotes inflammatory response through STING–NF-κB signaling activation in vitro.** RAW264.7 macrophages were stimulated with LPS (300 ng mL$^{-1}$) for 16 hours. (*A*) Relative mRNA levels of IL1β, IL6, TNF-α, and MCP-1 in Vec-SCAP and SCAPi-RAW264.7 cells (n = 5). (*B*) Relative mRNA levels of IL1β, IL6, TNF-α, and MCP-1 in NC-SCAP and OE-SCAP RAW264.7 cells (n = 5). (*C*) Protein levels of P-P65, P65, and SCAP in RAW264.7 cells (n = 3). (*D*) Protein levels of P65 in cytosolic and nuclear fractions (n = 3). Immunofluorescence staining of p65 nuclear translocation in SCAPi-RAW264.7 cells (*E*) and OE-SCAP RAW264.7 cells (*F*) (n = 3). (*G*) Protein levels of STING, P-TBK1, TBK1, IKKα, IKKβ, P-IKKα/β, IκBα, and P-IκBα in RAW264.7 cells (n = 3). Data are expressed as mean ± SD. **P* < .05; ***P* < .01; ****P* < .0001; ns, nonsignificant (2-tailed unpaired *t* test in bar graphs).

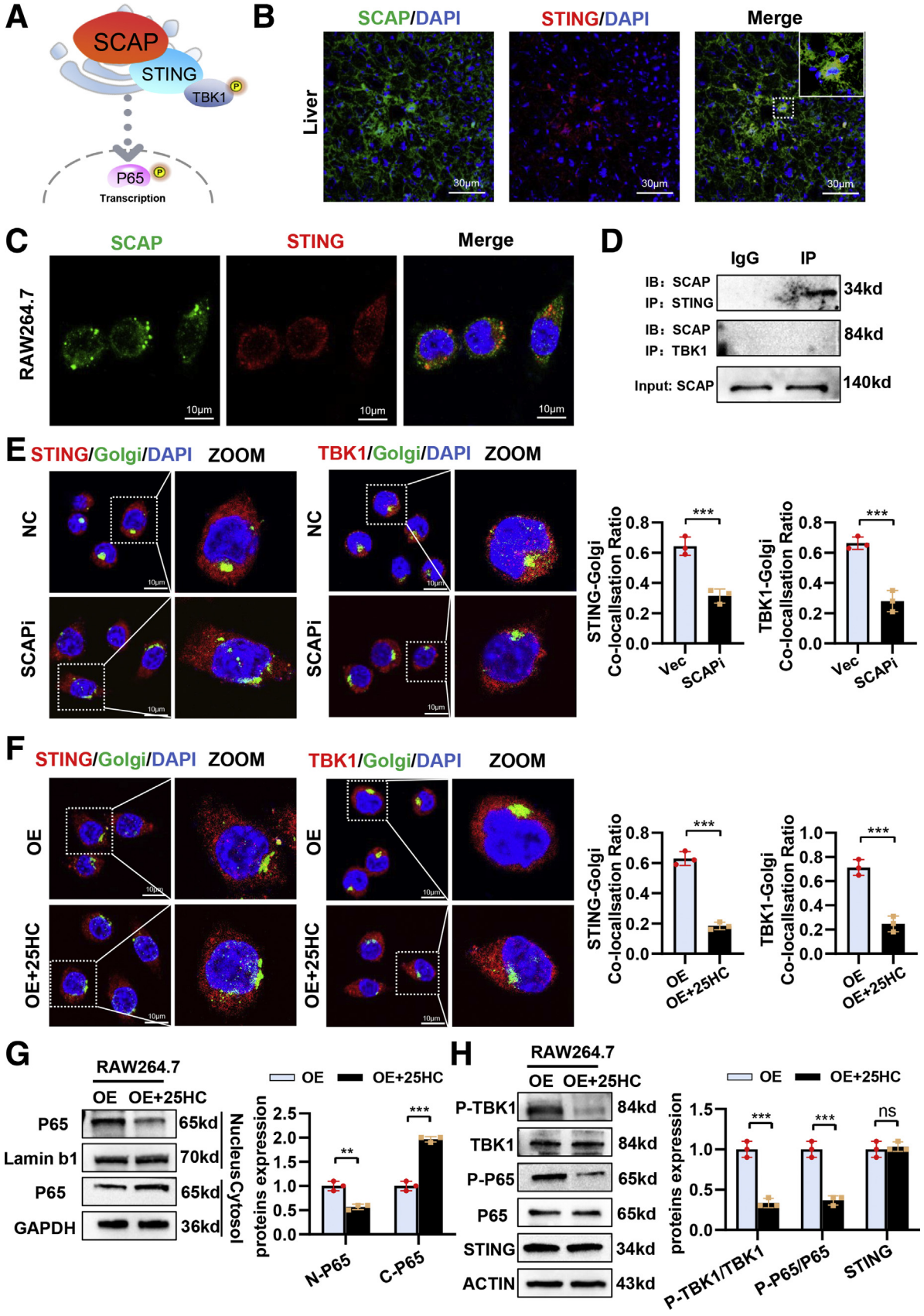
A
SCAP
STING
TBK1
P65
Transcription
B
SCAP/DAPI
STING/DAPI
Merge
Liver
30μm
C
SCAP
STING
Merge
RAW264.7
10μm
D
IgG
IP
IB：SCAP
IP：STING
34kd
IB：SCAP
IP：TBK1
84kd
Input: SCAP
140kd
E
STING/Golgi/DAPI ZOOM
TBK1/Golgi/DAPI ZOOM
NC
SCAPi
STING-Golgi Co-locallsation Ratio
TBK1-Golgi Co-locallsation Ratio
Vec
SCAPi
***
F
STING/Golgi/DAPI ZOOM
TBK1/Golgi/DAPI ZOOM
OE
OE+25HC
STING-Golgi Co-locallsation Ratio
TBK1-Golgi Co-locallsation Ratio
G
RAW264.7
OE OE+25HC
P65
Lamin b1
P65
GAPDH
65kd
70kd
65kd
36kd
Nucle
Cytosol
proteins expression
N-P65
C-P65
**
***
H
RAW264.7
OE OE+25HC
P-TBK1
TBK1
P-P65
P65
STING
ACTIN
84kd
84kd
65kd
65kd
34kd
43kd
P-TBK1/TBK1
P-P65/P65
STING
ns

supplemented with 10% fetal bovine serum (FBS) and 100 U/mL penicillin-streptomycin. Human hepatocellular carcinoma HepG2 cells were grown in Dulbecco modified Eagle medium (DMEM) supplemented with 10% FBS and 100 U/mL penicillin-streptomycin.

3T3-L1 pre-adipocytes were grown in DMEM containing 10% newborn calf serum and 1% antibiotics until confluence and induced to differentiation as previously described. Two days after confluence (day 0, D0), cells were induced by standard hormone cocktails. Briefly, cells were induced with DMEM containing 0.5 mmol/L isobutylmethylxanthine (ST1398; Beyotime), 1 $\mu$mol/L dexamethasone (ST1258; Beyotime), 10 $\mu$g/mL insulin (I6634; Sigma-Aldrich, St Louis, MO), and 10% FBS for 3 days. At the end of day 3, cells treated with DMEM supplemented only with 10 $\mu$g/mL insulin and 10% FBS and replenished every other day. On day 10, mature adipocytes were harvested for further experiments.

## Overexpression of SCAP

Lentivirus containing the mouse full-length cDNA of SCAP was purchased from Obio Technology (Shanghai, China). The lentiviruses were transfected into RAW264.7 at a multiplicity of infection of 30 and THP-1 at a multiplicity of infection of 50. Cells infected with empty lentivirus served as normal expression controls.

## siRNA Transfection

siRNAs against human SCAP (sense: 5′-CCUCCUGGCAG UAGAUGUAdTdT-3′, antisense: 5′-UACAUCUACUGCC AGGAGGdTdT-3′), mouse SCAP (sense: 5′-CCUCCUGGCAG UAGAUGUAdTdT-3′), antisense: (5′-UACAUCUACUGCCA GGAGGdTdT-3′), and siRNA negative control (Vec) were purchased from Obio Technology. SCAP was knocked down by transfecting 60%–70% confluent cells with siRNA by using Lipofectamine RNAi MAX (13778150; Invitrogen, Waltham, MA) according to the manufacturer's protocol.

## Co-culture

HepG2 hepatocytes were incubated for 24 hours with overexpression of SCAP/SCAPi or normal expression controls/Vec-SCAP THP-1 cells in the presence of LDL (200 $\mu$g/mL). 3T3-L1 mature adipocytes were incubated for 24 hours with overexpression of SCAP/SCAPi or normal expression controls/Vec-SCAP RAW264.7 cells in the presence of LDL (200 $\mu$g/mL).

## qRT-PCR

qRT-PCR was performed as described previously.[26] In brief, total RNA of the tissues and cells was extracted by TRIzol reagent (9109; Takara, Kusatsu, Japan). qRT-PCR was performed using the SYBR Green PCR Master Mix (9109; Takara) with specific primer sets shown in Tables 1 and 2. The relative expression of the genes was analyzed using the 2-ΔΔ Ct method, and $\beta$-actin was used as the internal reference gene.

## Oil Red O Staining

After treatment, the cells were collected, washed, and permeabilized with 4% paraformaldehyde for 20 minutes. Oil red O staining was performed according to the manufacturer's instructions (C0158S; Beyotime). Image analysis procedures were performed with Image J software.

## Immunofluorescence Staining and Confocal Microscopy

RAW264.7 cells were fixed with 4% paraformaldehyde (E672002; Sangon Biotech, Shanghai, China) for 15 minutes at room temperature and washed with phosphate-buffered saline (PBS) (E607008; Sangon Biotech) 3 times. After blocking, the cells were incubated with the primary antibodies for overnight at 4°C. The cells were then rinsed 3 times in PBS and incubated with the secondary antibody for 1–2 hours at 37°C. After washing with PBS, the cells were counterstained with DAPI (D9542; Sigma-Aldrich) for 5 minutes and visualized using fluorescent microscopy. The Pearson correlation (R value) and colocalization rate were analyzed from 3 different fields in each sample using Leica (Wetzlar, Germany) confocal microscope software. Antibodies are shown in Table 3.

## Biochemical Analysis

Serum samples and various tissues were collected from anesthetized mice, and the levels of total TG (A110-1-1; Nanjing JianCheng, Nanjing, China), cholesterol (A111-1-1; Nanjing JianCheng), high-density lipoprotein (HDL) cholesterol (A112-1-1; Nanjing JianCheng), and LDL (A113-1-1; Nanjing JianCheng) cholesterol were measured by enzymatic methods. Levels of IL1$\beta$ (EH001-48; Bioworlde), IL6 (EM004-96; Bioworlde), and TNF-$\alpha$ (ER006-96; Bioworlde) in mouse tissues were detected by using enzyme-linked immunosorbent assay kits according to the manufacturer's instructions.

**Figure 15.** (***See previous page***). **SCAP recruits STING and TBK1 to the Golgi and activates NF-$\kappa$B signaling.** RAW264.7 macrophages were stimulated with LPS (300 ng ml$^{-1}$) for 16 hours and 50 $\mu$mol/L 25-HC for 3 hours. (*A*) Schematic diagram of mechanisms by which macrophage SCAP activates STING–NF-$\kappa$B. Immunofluorescence staining of STING and SCAP in liver tissues (*B*) or RAW264.7 cells (*C*). (*D*) Immunoblotting of immunoprecipitation with anti-SCAP, anti-TBK1, and anti-STING in OE-SCAP RAW264.7 cells. (n = 3). (*E*) Immunofluorescence staining of STING, TBK1, and Golgi 97 in RAW264.7 cells treated with LPS (n = 3). (*F*) Immunofluorescence staining of STING, TBK1, and Golgi 97 in RAW264.7 cells treated with LPS (n = 3). (*G*) Protein levels of P65 in cytosolic and nuclear fractions (n = 3). (*H*) Protein levels of TBK1, P-TBK1, P-P65, P65, and STING in RAW264.7 cells (n = 3). Data are expressed as mean ± SD. **P* < .05; ***P* < .01; ****P* < .0001; ns, nonsignificant (2-tailed unpaired *t* test in bar graphs).

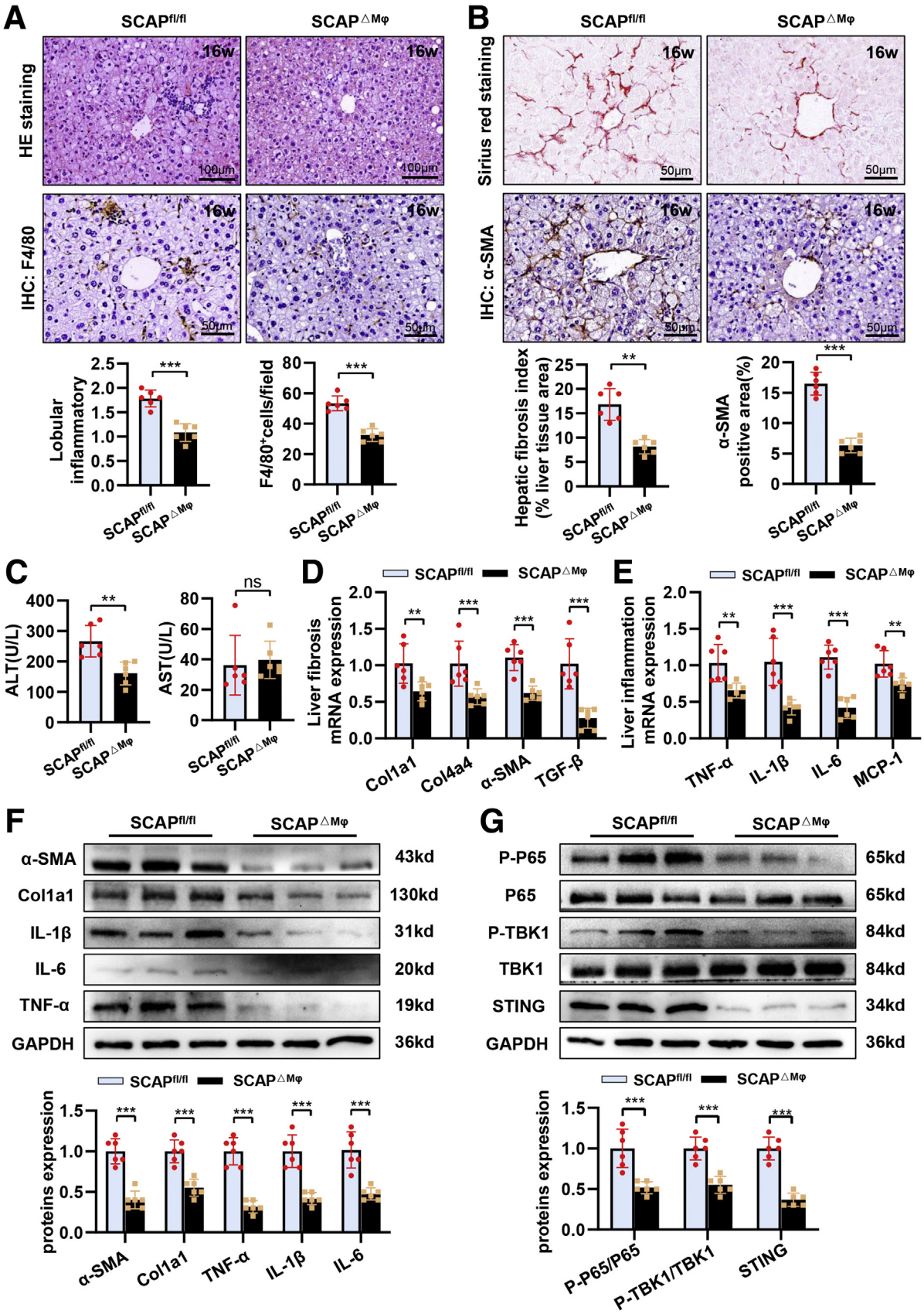
A
SCAP^fl/fl
SCAP^△Mφ
HE staining
IHC: F4/80
16w
100μm
50μm
Lobular inflammatory
F4/80+cells/field
B
Sirius red staining
IHC: α-SMA
Hepatic fibrosis index (% liver tissue area)
α-SMA positive area(%)
C
ALT(U/L)
AST(U/L)
ns
D
Liver fibrosis mRNA expression
Col1a1
Col4a4
α-SMA
TGF-β
E
Liver inflammation mRNA expression
TNF-α
IL-1β
IL-6
MCP-1
F
α-SMA 43kd
Col1a1 130kd
IL-1β 31kd
IL-6 20kd
TNF-α 19kd
GAPDH 36kd
proteins expression
G
P-P65 65kd
P65 65kd
P-TBK1 84kd
TBK1 84kd
STING 34kd
GAPDH 36kd
P-P65/P65
P-TBK1/TBK1
STING

**Table 1.** Information on Primers (Mouse) Used in This Study

| mRNA | Forward (5′-3′) | Reverse (5′-3′) |
|---|---|---|
| $\beta$-actin | CCTGAGGCTCTTTTCCAGCC | TAGAGGTCTTTACGGATGTCAACGT |
| TNF-$\alpha$ | CCTGTAGCCCACGTCGTAG | GGGAGTAGACAAGGTACAACCC |
| IL1$\beta$ | GAAATGCCACCTTTTGACAGTG | TGGATGCTCTCATCAGGACAG |
| IL6 | TCTATACCACTTCACAAGTCGGA | GAATTGCCATTGCACAACTCTTT |
| MCP-1 | TTAAAAACCTGGATCGGAACCAA | GCATTAGCTTCAGATTTACGGGT |
| SCD1 | TTCTTGCGATACACTCTGGTGC | CGGGATTGAATGTTCTTGTCGT |
| SREBP2 | GCAGCAACGGGACCATTCT | CCCCATGACTAAGTCCTTCAACT |
| ACC1 | ATGGGCGGAATGGTCTCTTTC | TGGGGACCTTGTCTTCATCAT |
| FASN | GGAGGTGGTGATAGCCGGTAT | TGGGTAATCCATAGAGCCCAG |
| ATGL | GGATGGCGGCATTTCAGACA | CAAAGGGTTGGGTTGGTTCAG |
| HSL | TCCCTCAGTATCTAGGCCAGA | GGCTCATTTGGGAGACTTTGTTT |
| MGL | CGGACTTCCAAGTTTTTGTCAGA | GCAGCCACTAGGATGGAGATG |
| CD36 | TTGAAGGCATTCCCACGTATC | CGGACCCGTTGGCAAA |
| PLIN1 | GGGACCTGTGAGTGCTTCC | GTATTGAAGAGCCGGGATCTTTT |
| FATP1 | CGCTTTCTGCGTATCGTCTG | GATGCACGGGATCGTGTCT |
| FATP4 | ACTGTTCTCCAAGCTAGTGCT | GATGAAGACCCGGATGAAACG |
| FATP5 | CTACGCTGGCTGCATATAGATG | CCACAAAGGTCTCTGGAGGAT |

## Insulin Tolerance Test and Glucose Tolerance Test

After 16 hours of fasting, mice were accepted to a glucose tolerance test (GTT), receiving an intraperitoneal injection of glucose solution (1.5 g glucose per kg body weight). Blood was collected from the tail, and glucose was measured at 0, 15, 30, 60, and 120 minutes after injection using a handheld glucometer (Roche, Basel, Switzerland). For the intraperitoneal insulin tolerance test (ITT), mice were fasted for 6 hours and injected with insulin (0.75 U $kg^{-1}$).

## Adipose Tissue Macrophage Isolation

eWAT was collected into ice-cold PBS to remove debris. The tissue was mechanically dissociated by mincing and treated with 0.1% collagenase (C5138; Sigma-Aldrich) in PBS for 1 hour at 37°C with gentle agitation. Digested samples were centrifuged at 300*g* at 4°C for 5 minutes to separate adipocytes and nonparenchymal cells. The cell pellet was resuspended in red blood cell lysis buffer (C3702; Beyotime) at 4°C for 5 minutes, then washed with PBS, and centrifuged at 1000*g* at 4°C for 5 minutes to obtain macrophages.

## Liver Macrophage Isolation

Liver tissue was collected into ice-cold PBS to remove debris. The tissue was mechanically dissociated by mincing and treated with 0.1% collagenase in PBS for 1 hour at 37°C with gentle agitation. The cell suspensions were filtered through a 70-$\mu$m nylon cell strainer. The filtered cells were centrifuged at 500*g* at 4°C for 5 minutes to separate nonparenchymal cells and hepatocytes. The cell pellet was resuspended in red blood cell lysis buffer at 4°C for 5 minutes, then washed with PBS, and centrifuged at 1000*g* at 4°C for 5 minutes to obtain macrophages.

## Flow Cytometry

The macrophages from eWAT and liver were isolated as described above. The isolated cells were fixed with 4% paraformaldehyde for 30 minutes. Adipose tissue macrophages were stained with anti-CD11C and anti-F4/80; liver macrophages were stained with anti-CD11b and anti-F4/80 for 30 minutes. Then cells were permeabilized with permeabilization wash buffer (abs9111; absin) and stained with anti-SCAP. Data acquisition was performed using the Airal2 flow cytometer (BD Biosciences, Franklin Lakes, NJ) and analyzed with Flowjo software (Tree Star Inc, Ashland, OR).

## Histology

Histology was done as described previously. Sections of 5-$\mu$m thickness were paraffin-embedded and prepared for H&E staining, immunohistochemistry, or immunofluorescence.

**Figure 16.** (***See previous page***). **Macrophage SCAP deletion ameliorates the degree of liver fibrosis in PD-fed mice.** (*A*) Representative pictures of H&E staining and immunohistochemical staining of $F4/80^+$ cells in mice fed a 16-week PD (n = 6). (*B*) Representative pictures of Sirius red staining and immunohistochemical staining of $\alpha$-SMA in mice fed a 16-week PD (n = 6). (*C*) Levels of ALT and aspartate aminotransferase in plasma (n = 6). (*D*) Relative mRNA levels of fibrosis in liver tissues (n = 6). (*E*) Relative mRNA levels of inflammation cytokine in liver tissues (n = 6). (*F*) Protein levels of $\alpha$-SMA, Col1a1, IL1$\beta$, IL6, TNF-$\alpha$, and MCP-1 in liver tissues (n = 6). (*G*) Protein levels of P-P65, P65, P-TBK1, TBK1, and STING in liver tissues (n = 6). Data are expressed as mean ± SD. **P* < .05; ***P* < .01; ****P* < .0001; ns, nonsignificant (2-tailed unpaired *t* test in bar graphs).

**Table 2.** Information on Primers (Human) Used in This Study

| mRNA | Forward (5′-3′) | Reverse (5′-3′) |
|---|---|---|
| β-actin | CCTGGCACCCAGCACAAT | GCCGATCCACACGGAGTA |
| TNF-α | GGAGAAGGGTGACCGACTCA | TGCCCAGACTCGGCAAAG |
| IL1β | TTCGACACATGGGATAACGAGG | TTTTTGCTGTGAGTCCCGGAG |
| IL6 | ACTCACCTCTTCAGAACGAATTG | CCATCTTTGGAAGGTTCAGGTTG |
| MCP-1 | CAGCCAGATGCAATCAATGCC | TGGAATCCTGAACCCACTTCT |
| SCD1 | TTCCTACCTGCAAGTTCTACACC | CCGAGCTTTGTAAGAGCGGT |
| SREBP2 | TCCGCCTGTTCCGATGTAC | TGCACATTCAGCCAGGTTCA |
| ACC1 | GGATCCGGCGCCTTACTT | CTCCGATCCACCTCATAGTTGAC |
| FASN | AAGGACCTGTCTAGGTTTGATGC | TGGCTTCATAGGTGACTTCCA |
| ATGL | ATGGTGGCATTTCAGACAACC | CGGACAGATGTCACTCTCGC |
| HSL | TCAGTGTCTAGGTCAGACTGG | AGGCTTCTGTTGGGTATTGGA |
| MGL | AATGCAGACGGACAGTACCTC | GAGCCAGCTCTTCATAGCGG |
| CD36 | TTCCTGCAGCCCAATGGT | TTGTCAGCCTCTGTTCCAACTG |
| PLIN1 | CCATGTCCCTATCAGATGCCC | CTGGTGGGTTGTCGATGTC |
| FATP1 | CTTCGATGGCTATGTCAGCGA | AGCACGTCACCTGAGAGGTAG |
| FATP4 | GTACTCAAGCAGTGTAGCCAAC | CTCATTGCGGTTCTCCATGAA |
| FATP5 | GCTTCGGTCCTATTCGGATCT | CAGCGCCCCACATAGTTGA |

## Co-IP and Western Blotting

RAW264.7 cells were lysed in NP40 buffer (P0013F; Beyotime) supplemented with protease and phosphatase inhibitors. After 2 hours of incubation with agarose beads, the cell lysates were incubated overnight with immunoglobulin G or anti-SCAP antibody. The immunocomplexes were washed 3 times with PBS and collected proteins from the magnetic beads. Finally, the proteins were detected by Western blotting analysis.

Western blotting was performed as described previously.[21] Total proteins were separated by sodium dodecyl sulfate-polyacrylamide gel electrophoresis and then transferred to a polyvinylidene difluoride membrane (IEVH85R; Millipore, Burlington, MA). Then, the membranes were blocked with 3% bovine serum albumin for 1 hour. After primary antibodies overnight incubation, the membranes were incubated with horseradish peroxidase–labeled corresponding secondary antibodies. Finally, detection was visualized by using the ECL chemical luminescent detection kit (Bio-Rad, Hercules, CA), and the bands were further analyzed using Quantity One software. Antibodies are shown in Table 3.

**Table 3.** Information About Antibodies

| Name | Source | Product number |
|---|---|---|
| SCAP | Abcam | ab153933 |
| P65 | Santa Cruz | sc-8008 |
| P-P65 | Santa Cruz | sc-136548 |
| IKKα | Santa Cruz | sc-52932 |
| IKKβ | Santa Cruz | sc-8014 |
| P-IKKα/β | Affinity Biosciences | AF3013 |
| IκB-α | Santa Cruz | sc-4094 |
| P-IκB-α | Santa Cruz | sc-8404 |
| Lamin b1 | Proteintech | 12987-1-AP |
| TBK1 | Proteintech | 67211-1-Ig |
| P-TBK1 | Beyotime | AF5959 |
| STING | Proteintech | 66680-1-Ig |
| Golgin 97 | Abcam | ab84340 |
| GAPDH | Proteintech | 10494-1-AP |
| Col1a1 | Wanleibio | WL0088 |
| IL1β | Proteintech | 16806-1-AP |
| TNF-α | Proteintech | 17590-1-AP |
| IL6 | Proteintech | 21865-1-AP |
| α-SMA | Proteintech | 14395-1-AP |
| ACTIN | Proteintech | 20536-1-AP |

## Statistical Analysis

The results are reported as means ± standard deviation (SD). Differences between groups were determined using 2-tailed Student $t$ test, and statistical significance in body weight and GTT and ITT curves were tested by two-way analysis of variance, using GraphPad Prism 8 (San Diego, CA) software. $P < .05$ was considered significant.

# References

1. Wang AY, Dhaliwal J, Mouzaki M. Lean non-alcoholic fatty liver disease. Clinical Nutrition (Edinburgh, Scotland) 2019;38:975–981.
2. Mellinger JL, Pencina KM, Massaro JM, Hoffmann U, Seshadri S, Fox CS, O'Donnell CJ, Speliotes EK. Hepatic steatosis and cardiovascular disease outcomes: an analysis of the Framingham Heart Study. J Hepatol 2015; 63:470–476.

3. Sinn DH, Gwak GY, Park HN, Kim JE, Min YW, Kim KM, Kim YJ, Choi MS, Lee JH, Koh KC, Paik SW, Yoo BC. Ultrasonographically detected non-alcoholic fatty liver disease is an independent predictor for identifying patients with insulin resistance in non-obese, non-diabetic middle-aged Asian adults. Am J Gastroenterol 2012; 107:561–567.
4. Ye Q, Zou BY, Yeo YH, Li J, Huang DQ, Wu YK, Yang HL, Liu CL, Kam LY, Tan XXE, Chien N, Trinh S, Henry L, Stave CD, Hosaka T, Cheung RC, Nguyen MH. Global prevalence, incidence, and outcomes of non-obese or lean non-alcoholic fatty liver disease: a systematic review and meta-analysis. Lancet Gastroenterol 2020; 5:739–752.
5. Das K, Das K, Mukherjee PS, Ghosh A, Ghosh S, Mridha AR, Dhibar T, Bhattacharya B, Bhattacharya D, Manna B, Dhali GK, Santra A, Chowdhury A. Nonobese population in a developing country has a high prevalence of nonalcoholic fatty liver and significant liver disease. Hepatology 2010;51:1593–1602.
6. Fan JG, Kim SU, Wong VW. New trends on obesity and NAFLD in Asia. J Hepatol 2017;67:862–873.
7. Younossi ZM, Stepanova M, Negro F, Hallaji S, Younossi Y, Lam B, Srishord M. Nonalcoholic fatty liver disease in lean individuals in the United States. Medicine 2012;91:319–327.
8. Iacobini C, Pugliese G, Fantauzzi CB, Federici M, Menini S. Metabolically healthy versus metabolically unhealthy obesity. Metabolism 2019;92:51–56.
9. Feng RN, Du SS, Wang C, Li YC, Liu LY, Guo FC, Sun CH. Lean-non-alcoholic fatty liver disease increases risk for metabolic disorders in a normal weight Chinese population. World J Gastroenterol 2014; 20:17932–17940.
10. Zou B, Yeo YH, Nguyen VH, Cheung R, Ingelsson E, Nguyen MH. Prevalence, characteristics and mortality outcomes of obese, nonobese and lean NAFLD in the United States, 1999-2016. J Intern Med 2020; 288:139–151.
11. Wang QY, You H, Ou XJ, Zhao XY, Sun YM, Wang M, Wang P, Wang Y, Duan WJ, Wang XM, Wu SS, Kong YY, Saxena R, Gouw ASH, Jia JD. Non-obese histologically confirmed NASH patients with abnormal liver biochemistry have more advanced fibrosis. Hepatol Int 2019; 13:766–776.
12. Denkmayr L, Feldman A, Stechemesser L, Eder SK, Zandanell S, Schranz M, Strasser M, Huber-Schonauer U, Buch S, Hampe J, Paulweber B, Lackner C, Haufe H, Sotlar K, Datz C, Aigner E. Lean patients with non-alcoholic fatty liver disease have a severe histological phenotype similar to obese patients. J Clin Med 2018;7(12).
13. Feldman A, Eder SK, Felder TK, Kedenko L, Paulweber B, Stadlmayr A, Huber-Schonauer U, Niederseer D, Stickel F, Auer S, Haschke-Becher E, Patsch W, Datz C, Aigner E. Clinical and metabolic characterization of lean Caucasian subjects with non-alcoholic fatty liver. Am J Gastroenterol 2017; 112:102–110.
14. Despres JP, Lemieux I, Bergeron J, Pibarot P, Mathieu P, Larose E, Rodes-Cabau J, Bertrand OF, Poirier P. Abdominal obesity and the metabolic syndrome: contribution to global cardiometabolic risk. Arterioscler Thromb Vasc 2008;28:1039–1049.
15. Musso G, Gambino R, De Michieli F, Cassader M, Rizzetto M, Durazzo M, Faga E, Silli B, Pagano G. Dietary habits and their relations to insulin resistance and postprandial lipemia in nonalcoholic steatohepatitis. Hepatology 2003;37:909–916.
16. Yasutake K, Nakamuta M, Shima Y, Ohyama A, Masuda K, Haruta N, Fujino T, Aoyagi Y, Fukuizumi K, Yoshimoto T, Takemoto R, Miyahara T, Harada N, Hayata F, Nakashima M, Enjoji M. Nutritional investigation of non-obese patients with non-alcoholic fatty liver disease: the significance of dietary cholesterol. Scand J Gastroenterol 2009;44:471–477.
17. Younes R, Govaere O, Petta S, Miele L, Tiniakos D, Burt A, David E, Vecchio FM, Maggioni M, Cabibi D, McLeod D, Pareja MJ, Fracanzani AL, Aller R, Rosso C, Ampuero J, Gallego-Durán R, Armandi A, Caviglia GP, Zaki MYW, Liguori A, Francione P, Pennisi G, Grieco A, Birolo G, Fariselli P, Eslam M, Valenti L, George J, Romero-Gómez M, Anstee QM, Bugianesi E. Caucasian lean subjects with non-alcoholic fatty liver disease share long-term prognosis of non-lean: time for reappraisal of BMI-driven approach? Gut 2021.
18. Pindjakova J, Sartini C, Lo Re O, Rappa F, Coupe B, Lelouvier B, Pazienza V, Vinciguerra M. Gut dysbiosis and adaptive immune response in diet-induced obesity vs systemic inflammation. Front Microbiol 2017;8.
19. Goldstein JL, DeBose-Boyd RA, Brown MS. Protein sensors for membrane sterols. Cell 2006;124:35–46.
20. Guo C, Chi Z, Jiang D, Wang D. Cholesterol homeostatic regulator SCAP-SREBP2 integrates NLRP3 inflammasome activation and cholesterol biosynthetic signaling in macrophages. Eur J Immunol 2019;49: 1278–1279.
21. Chen YX, Ku H, Zhao L, Wheeler DC, Li LC, Li Q, Varghese Z, Moorhead JF, Powis SH, Huang AL, Ruan XZ. Inflammatory stress induces statin resistance by disrupting 3-hydroxy-3-methylglutaryl-CoA reductase feedback regulation. Arterioscler Thromb Vasc 2014; 34:365–376.
22. Ye Q, Chen YX, Lei H, Liu Q, Moorhead JF, Varghese Z, Ruan XZ. Inflammatory stress increases unmodified LDL uptake via LDL receptor: an alternative pathway for macrophage foam-cell formation. Inflamm Res 2009; 58:809–818.
23. Ma KL, Ruan XZ, Powis SH, Chen Y, Moorhead JF, Varghese Z. Inflammatory stress exacerbates lipid accumulation in hepatic cells and fatty livers of apolipoprotein E knockout mice. Hepatology 2008; 48:770–781.
24. Li LC, Varghese Z, Moorhead JF, Lee CT, Chen JB, Ruan XZ. Cross-talk between TLR4-MyD88-NF-$\kappa$B and SCAP-SREBP2 pathways mediates macrophage foam cell formation. Am J Physiol Heart Circ Physiol 2013; 304:H874–H884.

25. Ouyang N, Gan H, He Q, Lei H, Wang SY, Liu Q, Zhou C. Dysfunction of cholesterol sensor SCAP promotes inflammation activation in THP-1 macrophages. Exp Cell Res 2018;367:162–169.
26. Li DY, Liu MH, Li Z, Zheng G, Chen AM, Zhao L, Yang P, Wei L, Chen YX, Ruan XZ. Sterol-resistant SCAP overexpression in vascular smooth muscle cells accelerates atherosclerosis by increasing local vascular inflammation through activation of the NLRP3 inflammasome in mice. Aging Dis 2021;12:747–763.
27. Perkins ND. The diverse and complex roles of NF-$\kappa$B subunits in cancer. Nature Reviews Cancer 2012;12:121–132.
28. Zhao P, Wong KI, Sun XL, Reilly SM, Uhm M, Liao ZJ, Skorobogatko Y, Saltiel AR. TBK1 at the crossroads of inflammation and energy homeostasis in adipose tissue. Cell 2018;172:731–743.e12.
29. Luo XJ, Li HG, Ma LQ, Zhou J, Guo X, Woo SL, Pei Y, Knight LR, Deveau M, Chen YM, Qian XX, Xiao XQ, Li QF, Chen XB, Huo YQ, McDaniel K, Francis H, Glaser S, Meng FY, Alpini G, Wu CD. Expression of STING is increased in liver tissues from patients with NAFLD and promotes macrophage-mediated hepatic inflammation and fibrosis in mice. Gastroenterology 2018;155:1971–1984.e4.
30. Yu YS, Liu Y, An WS, Song JW, Zhang YF, Zhao XX. STING-mediated inflammation in Kupffer cells contributes to progression of nonalcoholic steatohepatitis. J Clin Invest 2019;129:546–555.
31. Li N, Zhou H, Wu H, Wu Q, Duan M, Deng W, Tang Q. STING-IRF3 contributes to lipopolysaccharide-induced cardiac dysfunction, inflammation, apoptosis and pyroptosis by activating NLRP3. Redox Biology 2019;24:101215.
32. Motwani M, Pesiridis S, Fitzgerald KA. DNA sensing by the cGAS-STING pathway in health and disease. Nature Reviews Genetics 2019;20:657–674.
33. Tojima Y, Fujimoto A, Delhase M, Chen Y, Hatakeyama S, Nakayama K, Kaneko Y, Nimura Y, Motoyama N, Ikeda K, Karin M, Nakanishi M. NAK is an IkappaB kinase-activating kinase. Nature 2000;404:778–782.
34. Vergnes L, Phan J, Strauss M, Tafuri S, Reue K. Cholesterol and cholate components of an atherogenic diet induce distinct stages of hepatic inflammatory gene expression. J Biol Chem 2003;278:42774–42784.
35. Abate N. Adipocyte maturation arrest: a determinant of systemic insulin resistance to glucose disposal. J Clin Endocr Metab 2012;97:760–763.
36. Samuel VT, Shulman GI. The pathogenesis of insulin resistance: integrating signaling pathways and substrate flux. J Clin Invest 2016;126:12–22.
37. van Hall G, Steensberg A, Sacchetti M, Fischer C, Keller C, Schjerling P, Hiscock N, Moller K, Saltin B, Febbraio MA, Pedersen BK. Interleukin-6 stimulates lipolysis and fat oxidation in humans. J Clin Endocr Metab 2003;88:3005–3010.
38. Yang X, Zhang X, Heckmann BL, Lu X, Liu J. Relative contribution of adipose triglyceride lipase and hormone-sensitive lipase to tumor necrosis factor-$\alpha$ (TNF-$\alpha$)-induced lipolysis in adipocytes. J Biol Chem 2011;286:40477–40485.
39. Smith K. Liver disease: Kupffer cells regulate the progression of ALD and NAFLD. Nature Reviews Gastroenterology Hepatology 2013;10:503.
40. Koyama Y, Brenner DA. Liver inflammation and fibrosis. J Clin Invest 2017;127:55–64.
41. Ning L, Wei W, Wenyang J, Rui X, Qing G. Cytosolic DNA-STING-NLRP3 axis is involved in murine acute lung injury induced by lipopolysaccharide. Clinical and Translational Medicine 2020;10:e228.
42. Piperno GM, Naseem A, Silvestrelli G, Amadio R, Caronni N, Cervantes-Luevano KE, Liv N, Klumperman J, Colliva A, Ali H, Graziano F, Benaroch P, Haecker H, Hanna RN, Benvenuti F. Wiskott-Aldrich syndrome protein restricts cGAS/STING activation by dsDNA immune complexes. JCI insight 2020;5(17).
43. Shang G, Zhang C, Chen ZJ, Bai XC, Zhang X. Cryo-EM structures of STING reveal its mechanism of activation by cyclic GMP-AMP. Nature 2019;567:389–393.

**Received January 25, 2022. Accepted March 24, 2022.**

**Correspondence**
Address correspondence to: Danyang Li, PhD or Yaxi Chen, PhD, Centre for Lipid Research & Key Laboratory of Molecular Biology for Infectious Diseases (Ministry of Education), Institute for Viral Hepatitis, Department of Infectious Diseases, Second Affiliated Hospital, Chongqing Medical University, 400016 Chongqing, China. e-mail: lidycq@cqmu.edu.cn; chenyaxi@cqmu.edu.cn; fax: +86-23-68486780.

**CRediT Authorship Contributions**

Xinyu Huang (Conceptualization: Equal; Data curation: Lead; Formal analysis: Lead; Investigation: Lead; Writing – original draft: Lead; Writing – review & editing: Equal)

Yingcheng Yao (Data curation: Equal; Formal analysis: Equal; Investigation: Equal; Methodology: Equal)

Xiaoli Hou (Data curation: Equal; Formal analysis: Supporting)

Li Wei (Data curation: Supporting; Project administration: Supporting)

Yunhan Rao (Data curation: Supporting; Investigation: Supporting; Project administration: Supporting)

Yu Su (Data curation: Supporting)

Guo Zheng (Data curation: Supporting; Investigation: Supporting)

Xiong Z. Ruan (Writing – review & editing: Equal)

Danyang Li (Conceptualization: Equal; Formal analysis: Supporting; Funding acquisition: Supporting; Investigation: Supporting; Methodology: Supporting; Writing – review & editing: Equal)

Yaxi Chen (Conceptualization: Lead; Formal analysis: Supporting; Funding acquisition: Lead; Project administration: Lead; Software: Lead; Writing – review & editing: Lead)

**Conflicts of interest**
The authors disclose no conflicts.

**Funding**
Supported by the National Natural Science Foundation of China (82170586, 81900406); the Chongqing Research Program of Basic Research and Frontier Technology (cstc2020jcyj-zdxmX0007); the China Postdoctoral Science Foundation (Grant No.2019M663448); the Natural Science Foundation of Chongqing Province (Grant No. CSTC2019JCYJ-BSHX0094); Kuanren Talents Program of the Second Affiliated Hospital of Chongqing Medical University; and the 111 Project (No. D20028).